


Fall 11-15-2017

# Investigating Scalable Manufacturing of High-Conductivity Wires and Coatings From Ultra-Long Carbon Nanotubes

Pouria Khanbolouki

*University of New Mexico - Main Campus*

Follow this and additional works at: [https://digitalrepository.unm.edu/me\\_etds](https://digitalrepository.unm.edu/me_etds)

 Part of the [Electrical and Electronics Commons](#), [Materials Chemistry Commons](#), [Mechanical Engineering Commons](#), [Nanoscience and Nanotechnology Commons](#), and the [Other Materials Science and Engineering Commons](#)

---

## Recommended Citation

Khanbolouki, Pouria. "Investigating Scalable Manufacturing of High-Conductivity Wires and Coatings From Ultra-Long Carbon Nanotubes." (2017). [https://digitalrepository.unm.edu/me\\_etds/142](https://digitalrepository.unm.edu/me_etds/142)

This Thesis is brought to you for free and open access by the Engineering ETDs at UNM Digital Repository. It has been accepted for inclusion in Mechanical Engineering ETDs by an authorized administrator of UNM Digital Repository. For more information, please contact [disc@unm.edu](mailto:disc@unm.edu).

Pouria Khanbolouki

*Candidate*

---

Mechanical Engineering

*Department*

---

This thesis is approved, and it is acceptable in quality and form for publication:

*Approved by the Thesis Committee:*

Dr. Mehran Tehrani, Chairperson

---

Dr. Nathan Jackson

---

Dr. Mani Hossein-Zadeh

---

---

---

---

---

---

---

---

---

---

**Investigating Scalable Manufacturing of High-Conductivity Wires  
and Coatings From Ultra-Long Carbon Nanotubes**

by

**POURIA KHANBOLOUKI**

**BACHELOR OF SCIENCE IN MECHANICAL ENGINEERING**

**ISFAHAN UNIVERSITY OF TECHNOLOGY**

**July 2013**

**THESIS**

Submitted in Partial Fulfillment of the  
Requirements for the Degree of

**Master of Science  
Mechanical Engineering**

The University of New Mexico  
Albuquerque, New Mexico

**December 2017**

## **DEDICATION**

To my mom, for her endless care, encouragement, and sacrifice.

In loving memory of my dad, whose guidance continues to lead me in the right direction.

## ACKNOWLEDGMENTS

I would like to thank my adviser and mentor, Professor Mehran Tehrani for his patient guidance throughout the whole project, from understanding to execution. His advice has always allowed me to aim for the best in me and my work.

I would also like to thank Nekoda van de Werken from the Advanced Structural and Energy Materials Lab, the Mechanical Engineering Department at UNM for his contributions, consultations, and support in this project. I would also like to express my gratitude to Dr. Terry Holesinger from Materials Physics and Applications Division of Los Alamos National Laboratory for his guidance in the first steps of this project, and his candor and generosity in sharing his experience. Lastly, I would like to thank Dr. Amir Ali for performing the contact angle measurements.

Raman spectroscopy of samples was performed at the Center for Integrated Nanotechnologies, an Office of Science User Facility operated for the U.S. Department of Energy (DOE) Office of Science by Los Alamos National Laboratory (Contract DE-AC52-06NA25396) and Sandia National Laboratories (Contract DE-AC04-94AL85000).

# **INVESTIGATING SCALABLE MANUFACTURING OF HIGH- CONDUCTIVITY WIRES AND COATINGS FROM ULTRA- LONG CARBON NANOTUBES**

by

**Pouria Khanbolouki**

**B.S., Mechanical Engineering, Isfahan University of Technology, 2013**

**M.S., Mechanical Engineering, University of New Mexico, 2017**

## **ABSTRACT**

Carbon nanotubes (CNTs) are a promising candidate for next generation of electrical wirings and electromagnetic interference (EMI) shielding materials due to their exceptional mechanical and electrical properties. Wires and coatings from ultralong nanotubes that are highly crystalline, well-aligned and densely packed can achieve this goal. High-performance CNT conductors will be relatively lightweight and resistant to harsh conditions and therefore can potentially replace current conductors in many industries including aerospace, automotive, gas and oil.

This thesis investigates a new manufacturing approach, based on conventional solution coating and wire drawing methods, to fabricate high conductivity wires and coatings from ultra-long carbon nanotubes. This approach enables forming dense and aligned coatings of CNTs on various substrate wires. To achieve the carbon nanotube coating, millimeters long and vertically aligned multi-walled carbon nanotube arrays are first dispersed in sulfuric acid via mild shear mixing, forming CNT fibers. The resulting

fibers are subsequently solution coated onto a substrate wire (i.e., nylon and copper here) and the coating was subsequently drawn through a series of dies. During each drawing step, the CNT coated wire is passed through a wire drawing die to decrease the coating thickness and to coax the CNTs to align and pack. Effects of various processing parameters on the structure and resulting electrical conductivity of coated wires were investigated. By controlling processing parameters and number of dip coatings, both thin and thick coatings were formed on substrate wires; coatings accounting for up to 80% of the total wire cross-section were achieved. Microscopy and Raman spectroscopy were utilized to probe the structure of CNTs in the coatings. Adding short single-walled nanotubes to the ultra-long multi-walled ones in the coating solution resulted in 46.8% improvement in conductivity of the coatings. It was concluded that the continuous coating process introduced here can be used to manufacture high conductivity coatings and wires.

In chapter 1, the motivation behind this study is presented and structure of CNTs are explained. Chapter 2 reviews, in detail, CNT synthesis approaches and also our results on chemical vapor deposition of CNTs. Chapter 3 discusses advantages and disadvantages of different CNT wire and fiber manufacturing techniques, solution coated wires using our novel approach, and results of CNT coated copper and nylon wires. Electrical properties of the prepared wires and their structural characterization via Raman spectroscopy and scanning electron and light microscopies are discussed in chapters 4 and 5. Finally, a discussion of structure-property relationships of the CNT coated wires is presented in chapter 6.

## TABLE OF CONTENTS

Dedication .....	iii
Acknowledgments.....	iv
ABSTRACT.....	v
Table of Contents .....	vii
LIST OF FIGURES .....	ix
LIST OF TABLES .....	xiii
Chapter 1 : INTRODUCTION.....	1
1.1. CNT Structure and Properties .....	4
Chapter 2 : SYNTHESIS OF CARBON NANOTUBES .....	8
2.1. CNT Synthesis Approaches .....	8
2.2. Chemical Vapor Deposition (CVD).....	10
2.3. CNT Growth Mechanism.....	12
2.4. Synthesis of CNTs by Chemical Vapor Deposition.....	14
Chapter 3 : MANUFACTURING ALIGNED CNT STRUCTURES .....	20
3.1. Choice of CNT dispersion medium for CNTs .....	22
3.2. Other parameters affecting CNT dispersions .....	24
3.3. Experimental .....	28
CNT solution preparation .....	28
Dip-coating process .....	31
CNT coating / substrate interaction.....	35



Chapter 4 : ELECTRICAL CHARACTERIZATION OF WIRES AND COATINGS ...	41
4.1. Wire diameter measurements .....	41
4.2. Electrical Conductivity measurements at room temperature .....	43
Chapter 5 : STRUCTURAL CHARACTERIZATION OF CNT WIRES .....	52
5.1. Microscopy.....	52
5.2. Scanning Electron Microscopy .....	53
SEM of MWCNTs.....	53
SEM of CNT coated copper wires.....	54
SEM of CNT coated Nylon wires.....	57
5.3. Raman spectroscopy.....	58
Raman spectroscopy of MWCNTs.....	58
Polarized Raman spectroscopy .....	60
Chapter 6 : CONCLUSIONS AND FUTURE WORK .....	65
6.1. Conclusions .....	65
6.2. Future Work .....	66
Bibliography .....	68

## LIST OF FIGURES

Figure 1-1: Chirality table for single wall carbon nanotube. ....	5
Figure 2-1: Step-by-step preparation of the first substrate with photolithography and physical vapor deposition. ....	15
Figure 2-2: Profilometry of the photoresist layer on Si-SiO <sub>2</sub> substrate before the physical vapor deposition (i.e., sputtering) .....	16
Figure 2-3: a) Microscopy of the sputtered layer of alumina on Si-SiO <sub>2</sub> layer after the lift-off process. b) The substrate after PVD and lift-off processes. c) 3D AFM of the steps on the substrate. ....	16
Figure 2-4: The CVD setup used in this study. The setup consisted of three mass flow controllers, two furnaces, and a double bubbler system. ....	17
Figure 2-5: Reference CNT growth process .....	18
Figure 2-6: Catalyst layer annealing, and CNT nucleation and growth .....	18
Figure 2-7: One millimeter long CNT forest grew on a 0.5×0.5cm wafer using our recipe. ....	18
Figure 3-1: 2mm long MWCNT forest dispersed in 98% sulfuric acid with the aid of mechanical stirring, forming micron-size MWNT bundles.....	30
Figure 3-2: Left: Schematic for the dip-coating step of a copper wire in stirred solution. Right: Cross-section view of the dip-coating step with streamlines generated in the solution resulted from stirring.....	31
Figure 3-3: a) Schematic of CNT solution dip-coating process of Nylon wires. b) A cross-sectional view of the solution with streamlines generated in the solution while stirring.	32
Figure 3-4: CNT coated samples with nylon core .....	34

Figure 3-5: Schematic of the coating process of wires with dip-coating and densification of the coating in die drawing steps. SEM images of the substrate and coating are included to complement the schematics. ....	34
Figure 3-6: Contact angle measurements of water droplets on copper tape, untreated, and treated with 240grit sandpaper, 400grit sandpaper, Nitric acid, and Hydrochloric acid. .	37
Figure 3-7: Summary of contact angle measurements of water droplets on copper tape, untreated, and treated with 240grit sandpaper, 400grit sandpaper, Nitric acid, and Hydrochloric acid.....	37
Figure 3-8: Simple CNT coating adhesion test on a CNT coated copper substrate with adhesive tape. ....	38
Figure 3-9: Cross-sectional dark field microscopy images of CNT coated nylon wire (a), and sulfuric acid treated nylon wire (b). ....	39
Figure 4-1: Laser micrometer setup with custom-made sample holder for measuring the diameter of Nylon and Copper wire substrates as well as CNT coated composite wires.	41
Figure 4-2: Coating thickness range achieved for the composite wires (nylon and copper as substrates), coated at different shear mixing rates and subjected to die drawing. Average surface roughness of as coated and wire-drawn CNT coatings on copper and nylon substrates are also included.....	42
Figure 4-3: Experimental setup for electrical resistivity measurement: (a) top view; (b) isometric view. ....	47
Figure 4-4: Parallel resistance model for the copper-coated wires. This model assumes an infinite resistance at the copper-coating interface. ....	48

Figure 4-5: Four probe DC sweep resistance measurement of CNT coating, removed from copper substrate, in different current ranges. The voltage overflow happens at a value of  $\sim 5.2 \times 10^{-3} \text{A}$  while the voltage does not exceed values more than 120mV, which is far lower than the limits of the device. Experiments 13-18 in this set show that this phenomenon is reversible and does not affect the properties of the CNT coating. .... 50

Figure 4-6: Resistance vs. time measurements for composite CNT coated Nylon wire. The initial resistance of 14.65  $\Omega$  and final resistance of 13.36  $\Omega$  after 20 minutes. Method of measurement is 4 probe. .... 50

Figure 4-7: Electrical conductivity vs. CNT fiber area results from our studies and comparison with a selection of best results published for CNT fibers and wires. The data shown in this chart is for CNT coating cross-section only. .... 51

Figure 5-1: Scanning Electron Microscopy of pristine MWCNTs at a) 500K $\times$  magnification. b)  $\sim 200\times$  magnification. c) 20K $\times$  magnification. From the side view of the forest and d) 50K $\times$  magnification from top of the batch. .... 54

Figure 5-2: a and b) SEM images of General Nano MWCNT forests in different magnifications where entanglement is observable between nanotubes. c) a CNT coated copper wire after several wire drawing steps. d) the MWCNT bundles formed on the copper substrate and aligned in the direction of the long axis of the wire in c..... 55

Figure 5-3: a) Cross-section of CNT coated copper composite wire prepared with MWNT solution. b) A gap between CNT coating and copper substrate is visible in some areas of cross-sections. .... 56

Figure 5-4: Cross-sectional SEM images of CNT coated nylon wires without die drawing (a) and with die drawing (b). SEM of the surface of CNT coated nylon wires with no die drawing (c) and with die drawing (d). .....	57
Figure 5-5: Raman spectroscopy of the pristine MWCNT forests .....	59
Figure 5-6: Raman spectroscopy of MWCNT coating on nylon wire prepared from CNT/sulfuric acid solution dip-coating process. ....	60
Figure 5-7 - Polarized Raman spectroscopy of CNT coated Nylon sample from MWCNT solution as a function of measured angles 0, 20, 40, 50, 60, 90 degrees of polarization direction. ....	61
Figure 5-8: SEM (a) and polarized Raman spectroscopy(c) of aligned MWCNT sheet with zoomed in G-band intensities at 0,55, and 90 degree polarization direction compared to SEM (b) and polarized Raman spectroscopy (d) of an MWCNT coated nylon wire prepared by the method described in this work. ....	63
Figure 5-9: Polarized Raman spectroscopy of CNT coated Copper sample from MWCNT solution, with and without die drawing process.....	64
Figure 5-10: Polarized Raman spectroscopy of CNT coated nylon sample from MWCNT/SWCNT solution, with and without die drawing process .....	64
Figure 6-1: From individual MWCNTs to coatings of tens of microns in thickness. a) MWCNT forest at 300K× magnification. b) MWCNT fiber in sulfuric acid solution. c) Formation of MWCNT bundles on the surface of the coating. d) 69μm thick MWCNT coating on a 24AWG copper wire at 100× magnification. ....	66

## LIST OF TABLES

Table 1-1: Mechanical properties of carbon nanotubes and common structural materials	6
Table 3-1: Density, electrical and thermal conductivities of best results for dry-process and wet-processed CNT fibers in comparison to individual CNTs, Copper, and Aluminum .....	21
Table 3-2: Summary of the samples prepared for this study. 16 Samples (Average coating length of 15 cm per sample).....	40

## CHAPTER 1 : INTRODUCTION

Copper has been the choice material for electrical wirings since the early 19th century, and since then very few materials have been introduced to potentially replace it. Annealed copper is used for wirings, electrical contacts, and cables in city infrastructures, buildings, circuits and electronic circuitry, electric motors, aerospace industry, power generation and transmission, and telecommunication. This is due to the combination of copper's outstanding properties and its low price. Copper has one of the lowest electrical resistivity ratings of  $16.78 \text{ n}\Omega\cdot\text{m}$ . [1] It has an ultimate tensile strength of 200-350MPa, depending on the amount of cold work, and is ductile, which makes it suitable for metalworking and forming in different shape and size wires. [2, 3] Copper has also a high thermal conductivity,  $\sim 400 \text{ W/mK}$ , that facilitates dissipating heat from the system. [4] Other noteworthy properties are moderate corrosion and creep resistance, compatibility with different coatings and electrical insulators and solderability. [3] However, despite copper's fine properties and low cost, some industries such as aerospace, transportation and oil and gas, require wires with superior properties. While these advanced applications have been the driving force for finding replacement materials for copper, the US total electricity usage can be also lowered by 1% if copper were to be replaced by a CNT material that is only 33% more conducting than copper. [5]

Airframe wires in commercial and fighter aircraft need to possess great mechanical properties and operate in extreme environments, e.g., high temperatures. Braided metallic sheaths have been the solution for electromagnetic shielding and armor for different types of cables. There is an ever-increasing demand for embedding new

technologies in aircraft such as in-flight entertainment and wifi system.[6] As such, better data transfer in wires and cables as well as better ability to transfer more power to an increased number of devices is required in next generation of aircraft and satellites. These requirements will influence the total weight of the wires inside aircraft that will eventually result in more power and fuel consumption. Reducing the weight of power and data cables can be approached by two means. One addresses the design, and the other is to improve the material performance. It's noteworthy that modern aircraft usually feature up to 300 miles of wires.[6]

In oil and gas industry, there has always been an increasing demand for improved submersible pumps and wellhead pieces with increased power transmission and reliability without sacrificing the area available for existing footprint in deep water explorations.[7] Increased electrical transmissibility, as well as corrosion resistivity, enables more efficient, reliable and efficient dynamic mechanical performance in offshore drilling.[7]

For satellites, the launch cost is the single most critical concern and is directly correlated to the total weight of the satellite. For example, the average launch cost of communication satellites to orbit is \$10K per pound. The hundreds of kilograms of wires in satellites and rockets consist of various compositions of copper wires for different purposes. By reducing the total weight of wires consumed in any satellite and rocket by even a small percentage, and retaining the total current carrying capacity, the difference in the final cost can be millions of dollars. Of course, with any new wiring systems for the aerospace industry, there are more concerns than just the weight and ampacity, which can include the bend radius, high-temperature resistance, corrosion resistivity, etc. Higher



bend ratio gives designers more flexibility for a more compact aircraft design and assembly.

In some applications, advanced conducting wires should endure harsh conditions such as high levels of humidity or temperatures and be able to carry high currents (high ampacity).[8] Ampacity is defined as the current-carrying capacity of the conductor or the maximum amount of current it can carry in amperes before facing serious deteriorations. Ampacity depends on many factors including but not limited to the ambient temperature, the effective thermal resistance between conductor and surroundings and number of conductors in a raceway.[9] Copper's limited ampacity results in bulkier cables in many high current applications.

The quest for finding more cost-effective and efficient conductors has led to exploring other materials such as carbon nanotubes (CNT) for power distribution. Immediately after the discovery of carbon nanotubes in 1991 by Iijima [10], scientists were fascinated by their mechanical, electrical and thermal properties. A seamless cylinder of rolled up graphene sheet, a CNT, exhibits several microns of mean free path and ballistic transport of electrons.[11, 12] However, transferring the individual nanotube properties to the meso- and macro-scales have been a great challenge. Controlling the individual carbon nanotube characteristics such as radius, chirality, length, the number of walls during their synthesis as well as their alignment, morphology, and packing density throughout their post-synthesis processing has been a focus of intense research over the last two decades.

Nanotube's mechanical, electrical and thermal properties, make them a great candidate for the next generation of electrical wires in various systems that require

lightweight power or data cables, high current ratings, and corrosion and fatigue resistance. CNT wires can also be used in a variety of other applications such as electrochemical supercapacitors, sensors, and actuators. The two-dimensional structures of carbon nanotubes in the form of sheets have also been extensively studied for various applications such as thin film transistors, flexible electronics, transparent electrodes, displays, solar cells, energy storage, and supercapacitors. These 2D structures can be achieved through directly growing CNTs on the target substrate or by depositing the CNT layer on a target substrate from a solution in one or multiple step techniques such as Langmuir-Blodgett method, self-assembly, dip-coating, spin coating, drop casting, electrophoretic deposition, dielectrophoresis, spray coating, filtration method, Mayer rod, slot die, and gravure.[13] In the solution based coating techniques, CNT dispersion in the solution has a major influence on the final quality of the coating, which itself is determined by different parameters such as CNT quality, electrokinetic potential, bundle size and rheological properties.[14]

### **1.1. CNT Structure and Properties**

A nanotube can be visualized by rolling a graphene sheet in different directions. This rolling angle determines the electrical and optical properties of the nanotubes. This angle is referred to as the “chiral angle.” SWCNTs have diameters from 0.4 to 1.4 nm. MWCNTs consist of concentric SWCNT tubes with a spacing of 3.4Å and have diameters ranging 2-100nm. Shown by both theory and experiments, ballistic transport can occur in carbon nanotubes along their surfaces provided that the CNT is defect free.[12, 15]

The chirality, as shown in Figure 1-1, is defined by the angle between the chiral vector and the zigzag direction (n,0). All forms of nanotubes can be identified with (n,m) directional indices among which armchair is defined specifically having a 30° chiral angle and indices of (n,n) (Figure 1-1). CNT band gap can vary depending on its chirality from 0 to 2eV, resulting in semiconductor or metallic nanotubes. [16]

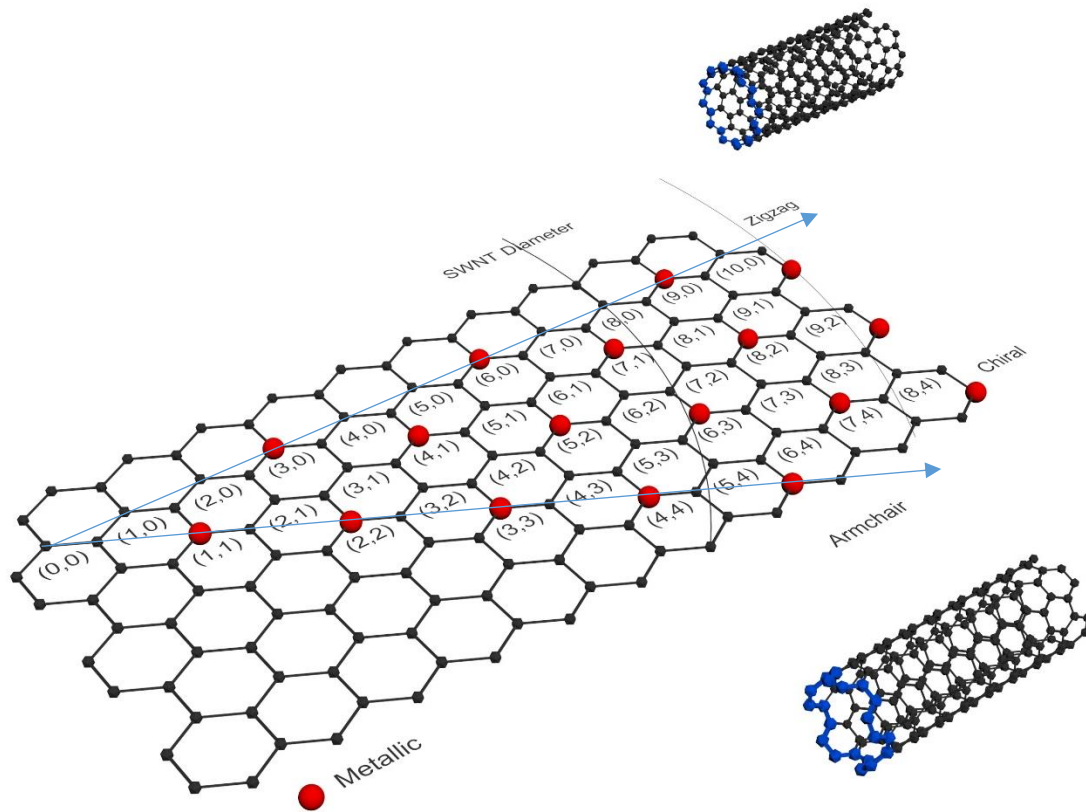


Figure 1-1: Chirality table for single wall carbon nanotube.

In addition to exceptional electrical properties, carbon nanotubes have a measured Young's modulus of 1.4TPa, 20-30% elongation to failure and high

stiffness.[17] The following table summarizes some comparisons between CNT and other materials properties.

Table 1-1: Mechanical properties of carbon nanotubes and common structural materials

<i>Material</i>	<i>Young's Modulus (GPa)</i>	<i>Tensile Strength (GPa)</i>	<i>Density (g cm<sup>-3</sup>)</i>
<i>CNTs</i>	300-950	10-200	0.7-1.7
<i>Steel</i>	210	0.4-2.0	7.8
<i>Kevlar</i>	60	3.6	1.44
<i>Copper</i>	120	0.22	8.92
<i>Aluminum</i>	70	0.3	2.70

In the following chapters, different CNT synthesis approaches are discussed. Parameters affecting CNT synthesis and termination mechanisms are explained. Chemical vapor deposition of CNTs is reviewed in more depth. Afterwards, Our attempt for CNT growth is explained from substrate preparation and CVD setup to parameters involved. In the third chapter, dry processing and wet processing of CNT wires and fibers are introduced. Advantages and disadvantages of various CNT fiber manufacturing techniques are discussed. Solution coating technique is further considered. Solution coating techniques for two-dimensional coatings is briefly introduced. Explanations on the choice of sulfuric acid for our process is provided, and different parameters are affecting the quality of CNT dispersions are introduced. Afterwards, our method for preparing CNT coatings for nylon and copper wire is thoroughly explained. This method is then used in a set of experiments for investigating the plausibility of this method for preparation of CNT conductive coatings. From chapter four, characterization of the CNT coatings begins. In chapter four, details about the method used for measuring dimensions and electrical conductivity of the coatings are included. Our results are then compared to the results from best publications on preparation of macro-scale CNT conductors. In

chapter five, Optical microscopy and Scanning Electron Microscopy images of CNT coatings are examined. Optical and SEM images taken are from side-view and cross-sectional view of the CNT coatings. Details about the process for preparing CNT coated wire cross-sections is also included. More detail about the adhesion of CNT coating to copper and nylon substrated are revealed. Later in this chapter, Raman spectroscopy results of pristine CNTs and CNT coatings are reviewed. Polarized Raman spectroscopy results from CNT coatings are compared with the SEM observations. In the last chapter, the results from this method are summarized, and conclusions are explained. More suggestions are provided to improve this method.

## CHAPTER 2 : SYNTHESIS OF CARBON NANOTUBES

Since their discovery, many attempts have been made to improve the quality, selectivity, yield, and length of carbon nanotubes, such as point-arc microwave plasma chemical vapor deposition (CVD),[18] floating catalyst CVD,[19] alcohol-assisted CVD,[20] molecular beam CVD,[21] hot filament CVD,[22] oxygen-hydrogen assisted CVD,[23] water assisted CVD,[24-27] fast-heating CVD [28] and horizontally aligned CVD grown CNTs (to up to 4cm long).[29] Among these synthesis methods, water assisted CVD seems to be a promising method for growing high-quality vertically aligned CNTs (VACNT) due to its cost-effectiveness and ease of implementation. Here, we survey CNT synthesis techniques.

### 2.1. CNT Synthesis Approaches

Before Iijima et al.[10] utilize an arc discharge method to synthesize CNTs,[30] scientists were using it to make fullerenes. In the arc discharge method, a DC is run between two vertical electrodes in the middle of a chamber, and an arc-discharge is generated. In this method, the thin anode electrode has small holes to be filled with a mixture of graphite and powder metals. The mixture gets vaporized by the laser beam in the tube at high temperatures (1200 °C) and in a flow of an inert gas. The multi-walled carbon nanotubes (SWCNT) grown by Iijima possess 2-50 walls and are deposited on a collector downstream the furnace.[31] This method has the advantage of high yields, but similar to the laser ablation method requires high energies and temperatures for sublimation of solid targets. In the laser ablation, the material is heated by a laser beam to

the point of sublimation and is separated from the source. In a research by Smalley et al.,[32] it was shown that carbon nanotubes could be formed and assembled on a substrate by laser ablation of a graphite source. Flame synthesis has also proven to be an effective method for growing CNT structures. Although, controlling the morphology and characteristics of as-grown CNTs in this method is more difficult than the other methods due to the complexities of mass transfer, heat transfer, and the dynamics of the flame.[33] With flame synthesis, the precursor is a mixture of reaction between a hydrocarbon and an oxidizer. The substrate is put in/on the flame, and the energy provided by the flame advances the synthesis of CNTs from the precursor on the catalytic particles over the substrate.[34] Trace of oxygen and hydrogen also has been proved in this method and are speculated to be influential in the promotion of CNT growth.[35, 36]

Each of these methods has advantages and disadvantages over one another. In comparison to chemical vapor deposition, which is the main focus of this chapter for CNT synthesis, the yield rate of arc discharge, laser ablation, and flame synthesis are low.[31, 37] It should be noted that higher nanotube qualities can be achieved via laser ablation because of the uniform conditions of growth under the laser beam. The highest achieved growth rates (not to be confused with yield!) for nanotube synthesis is by the flame method. All the synthesis methods require temperatures over 1000°C (4000°C in case of arc discharge) for the growth process to start.[31, 37] Chemical vapor deposition, on the other hand, utilizes temperatures in the range of 300-1200°C for the growth process.[31, 38]

## 2.2. Chemical Vapor Deposition (CVD)

CVD became an appealing choice for many research groups due to its low cost (due to its lower temperature), adaptability to the synthesis of a variety of structures, and scalability. In spite of these advantages, the method still faces the challenge of reproducibility.[31] In this process, nanotubes are formed via the decomposition of a mixture of gasses in high temperatures, and deposition of carbon on a catalyst particle. The precursor gasses commonly comprise alcohols,[39] aromatic compounds, hydrocarbons in the form of gas or liquid or even pure carbon.[38] Most frequent precursors used in this process are ethylene, acetylene, methane, carbon monoxide and ethanol. Through the years, many additives have been introduced inside the process for the purpose of promoting the growth such as water, hydrogen, and oxygen, or for doping the CNTs, such as nitrogen,[40] phosphorous,[41] and boron bearing gasses.[42] Many research groups came up with variations of CVD by changing multiple parameters or simply using variations of previous CVD techniques to achieve a higher controllability in CNT growth. Some of these methods include alcohol assisted-CVD,[43] water assisted-CVD (the super growth method),[44] floating catalyst CVD,[45] electric-field CVD,[46] low pressure CVD,[47] fluidized bed CVD,[48] plasma enhanced CVD, [49] hot filament CVD (Cold Wall),[50] horizontal tube CVD, point arc microwave plasma CVD,[42] and rotary tube furnace (Generally used for mass production).[51]

Although there are many synthesis parameters that affect the CNT structure, the catalyst is known to have a key impact. Thus preparation of the substrate becomes of great importance for controlling the final structure of the CNTs. Catalyst nanoparticles are prepared prior to the chemical deposition of carbon atoms. Variety of methods can be



used to form catalyst nanoparticles on substrates such as the sol-gel technique,[52] reduction of precursors,[52] evaporation of a solution on the substrate, self-assembly (micellar solution or reverse micelle method),[52] metal organic chemical vapor deposition,[48] dip-coating,[53] atomic layer deposition,[54] spin-coating, electroplating of nano-particles from a salt solution, contact print of nano-particle solutions, physical vapor sputtering, and finally evaporation techniques,[55] which have been shown to give promising results. One step preparation of catalyst nanoparticles can significantly improve the cost and rate of production of CNTs. To achieve this, both catalyst and precursors are introduced into the growth chamber at the same time, resulting in a continuous production of CNTs. CNTs are then collected downstream.

Iron-based catalysts are one of the most widely used ones for the synthesis of different CNT types. Cobalt- and nickel-based catalysts have also been utilized to grow MWCNTs and under certain conditions SWCNTs. Copper,[56] gold,[57] gadolinium, palladium,[58] platinum,[59] iridium,[60] silver,[61] rhenium, tungsten,[62] yttrium,[63] and molybdenum [64] are other elements that have been used to grow CNTs. Some elements are also used only as a part of multiple component catalysts or alloys such as molybdenum, magnesium, germanium, silicon and even carbon.[64, 65] Oxides of some of these elements can also be named as responsible for CNT growth, as shown in some studies.[66, 67]

Regardless of the synthesis method, CNTs are susceptible to containing impurities in the form of catalyst particles, amorphous carbons and other forms of carbon structures.[38] Post-processing and purification steps are therefore usually performed to

achieve high purity and consistent structures of CNTs depending on the CNT application.  
[68, 69]

### **2.3. CNT Growth Mechanism**

In 2013, Zhang et al.[70] produced a 550mm long CNT inside of a 35cm movable horizontal tube furnace with the total growth time of 120 mins. Precursors used consisted of CH<sub>4</sub>, H<sub>2</sub>, and H<sub>2</sub>O and growth temperature was set to 1100 °C. Recently, it was shown that with traditional water-assisted CVD, CNT forests could be grown to up to 2.17 cm.[71] Previously it was reported that water could prolong the lifetime of the catalyst nanoparticles.[44] A combination of parameters is involved in growing ultra-long CNT forests, but in theory, their synthesis can be continued as long as the catalyst nanoparticles are active. In addition, the catalyst lifetime depends on synthesis conditions such as temperature, pressure, annealing conditions, water vapor concentration, and carbon precursor.[38, 72, 73]

Understanding the CNT growth termination mechanism will enable us to improve the current methods to achieve more uniform CNT structures with higher yields. Carbon dissolution-diffusion-precipitation [74] (similar to the vapor-liquid-solid mechanism) is proposed to be one of the mechanisms involved in CNT growth. Some, however, believe that there is more than only one mechanism involved in their synthesis. The decomposition of the gaseous mixture is believed to occur mainly on the surface of catalytic nanoparticles, and the formation of the CNTs occur after diffusion of carbon atoms inside the catalysts.[75] Thus poisoning of the catalyst nanoparticles is believed to be one of the mechanisms involved in the termination of the process.[75] Nucleation of

the CNT By understanding the termination process, we would be able to control their growth more efficiently.

Studies show that deactivation of the catalyst occurs gradually [76] [77] [18] [78] or suddenly.[75, 79-81] An abrupt decrease in growth rate has also been shown in various studies. [82] [83-86] Some of these studies discuss the growth termination mechanisms. However, a universal explanation for this phenomenon does not currently exist.

The following factors individually or in combination with each other, are responsible for the growth termination.

- Diffusion rate of the carbon feedstock into CNT forest decreases with increasing the CNT length [26, 87]
- Diffusion rates of the carbon in and on the catalyst nanoparticles decreases with time [88]
- Catalyst poisoning and formation of carbon structures and oxides on or in catalyst nanoparticles [89-91]
- Ostwald ripening [92]
- Subsurface diffusion [93]
- CNT walls surface diffusion [94]
- Structure failure and van der Waals interactions of CNTs or covalent interaction of CNT dangling bonds [95]

Various parameters can affect the structure, morphology and other properties of the CNTs. As a result, different types of CNTs with dissimilar structures and properties have been discovered. Categorizing the CNTs by the number of concentric walls in the individual structures is one way of distinguishing them. In this category, we can mention

single wall, double wall, and multi-wall carbon nanotubes. Another way to categorize CNTs is based on the relative direction of the growth with respect to the substrate. It should be noted that orientation controlled growth of CNTs is another field of active research where different external forces such as gravitational, electric fields and magnetic fields are utilized to direct the growth direction.[96, 97] There are other variations of nanotube Such as carbon peapods, bamboo-shaped tubules, and branched CNTs.

#### **2.4. Synthesis of CNTs by Chemical Vapor Deposition**

It has been mentioned that every CVD process consists of two steps: 1) chemical reactions of precursor(s) and 2) deposition on a substrate. Different synthesis parameters can be controlled to achieve different types and morphologies, diameters, length and growth rate, chirality, and defects in nanotubes. This, in turn, results in different mechanical, electrical and thermal properties of nanotubes. Some of these key parameters are catalyst material, support material, surface roughness, catalyst layer thickness, support layer structure and thickness, growth Temperature, growth pressure, precursors, flow rates, flow profile, and feedstock pre-treatment.

To grow our ultra-long CNTs, three silicon wafers, 500 $\mu$ m thick, with a 500nm thermally grown SiO<sub>2</sub> were chosen. The first wafer was spin-coated with a photoresist, and by means of photolithography, a pattern was generated on it. This wafer was subsequently diced into pieces and used to measure the deposition rate of buffer and catalyst material using AJA ATC magnetron sputtering system. Aluminium oxide was used as the buffer and iron as the catalyst for the CVD nanotube synthesis. The height of the photoresist steps was probed by profilometry. After sputtering each of the 1 $\times$ 1cm

substrates with the desired thickness of iron or alumina, the photoresist was removed by a lift-off process, and the height of the steps was measured with a WITec Apyron atomic force microscope (AFM). This process is schematically shown in Figure 2-1. Figure 2-2 shows a typical an as-deposited photoresist.

After repeating the process with various parameters and acquiring a rate of deposition for aluminum oxide and iron, two wafers were sputtered by first, aluminum oxide and iron, respectively. Aluminium oxide was deposited at the rate of  $\sim 0.85\text{nm/min}$  for the duration of 12 minutes with an RF source power supply. Iron was sputtered using DC power supply at the rate of  $3.5\text{nm/min}$  for durations of less than two minutes. The wafers were then diced and used for CNT synthesis. Figure 2-3 shows the microscopy results and AFM of the layers generated by this method.

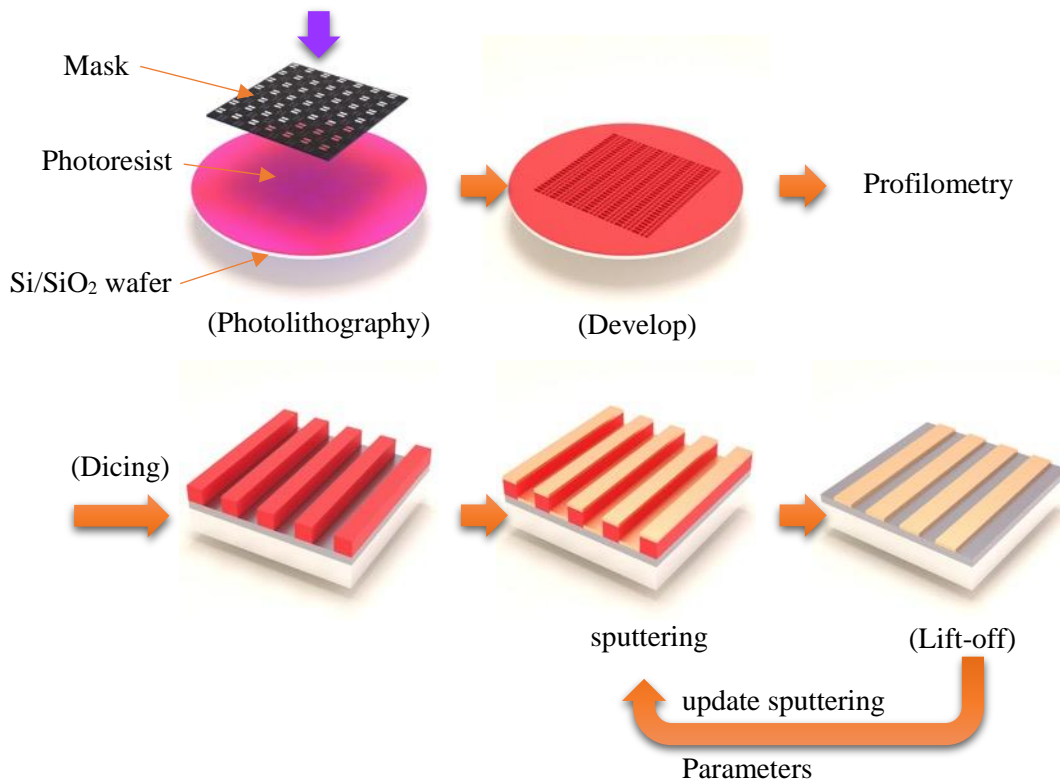


Figure 2-1: Step-by-step preparation of the first substrate with photolithography and physical vapor deposition.

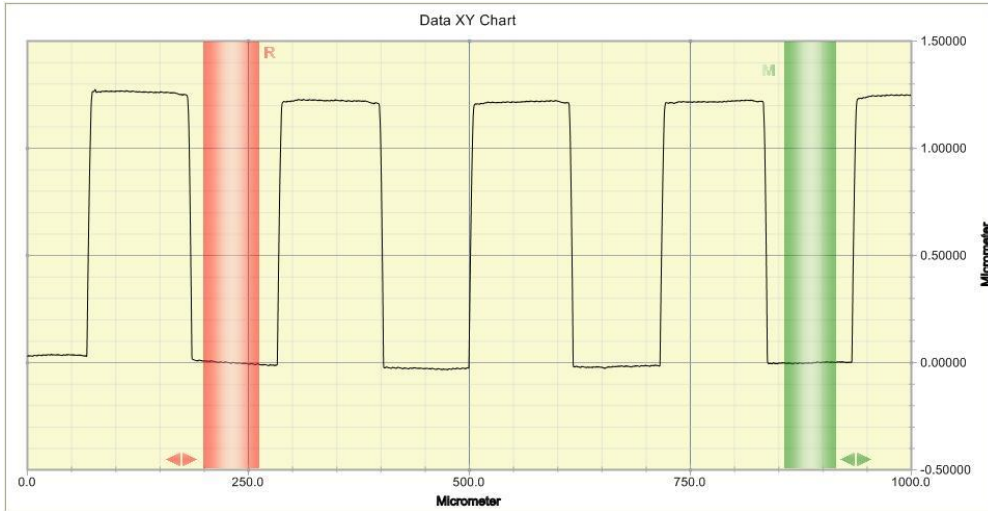


Figure 2-2: Profilometry of the photoresist layer on Si-SiO<sub>2</sub> substrate before the physical vapor deposition (i.e., sputtering)

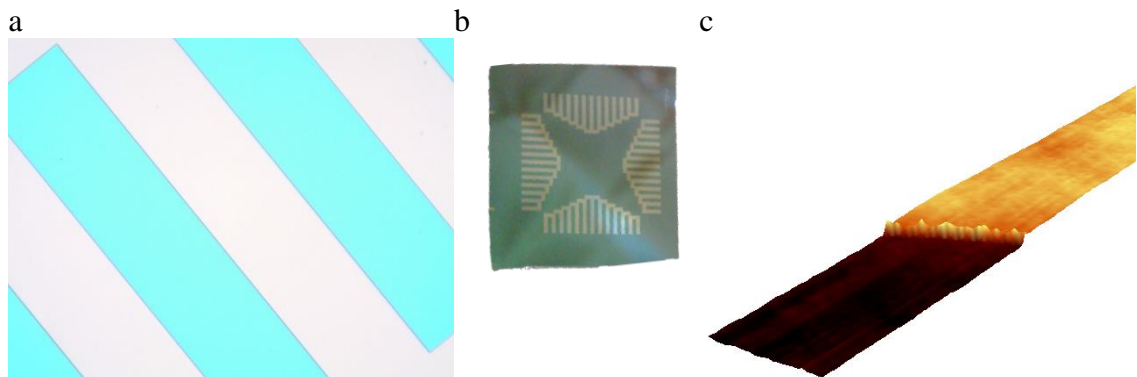


Figure 2-3: a) Microscopy of the sputtered layer of alumina on Si-SiO<sub>2</sub> layer after the lift-off process. b) The substrate after PVD and lift-off processes. c) 3D AFM of the steps on the substrate.

Our CVD setup, shown in Figure 2-4, is composed of a gas delivery system delivering high purity ethylene, argon, and a mixture of hydrogen and argon. Controllable delivery of the gasses is performed through three MKS mass flow controllers to two Lindberg Blue M horizontal tube furnaces in series with the total heated tube length of

120cm and a diameter of 25mm. The middle section of the tube is isolated so there would be minimum heat gradient between the furnaces. The downstream of the furnace is connected to a double bubbler system with oil as a trap. The accuracy of the mass flow controllers was checked by another set of flow controllers. The first furnace was used for purging as well as preheating of the reaction gasses.

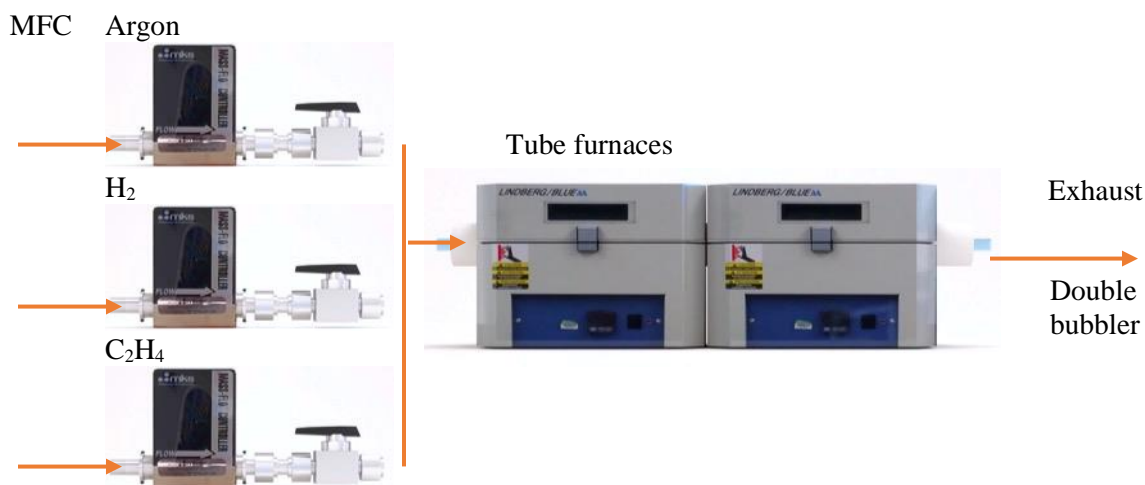


Figure 2-4: The CVD setup used in this study. The setup consisted of three mass flow controllers, two furnaces, and a double bubbler system.

Our growth procedure is shown in Figure 2-5. The process starts by placing a substrate (coated with the buffer and catalyst layers) in the middle of the first furnace operating at 150 °C. The tube was purged with an Ar/H<sub>2</sub> mixture for 30 minutes. The substrate is subsequently pushed into the second furnace, operating at 760°C, by means of a pushing rod. After 15 minutes of Ar/H<sub>2</sub> flow, ethylene was introduced. The iron layer breaks into catalytic nanoparticles during the initial annealing stage (Figure 2-6-b). At the end of growth (Figure 2-6-c), the ethylene feed was stopped, and samples were removed

after the furnaces cool down to below 150°C. Structure and quality of samples were investigated using SEM and Raman.

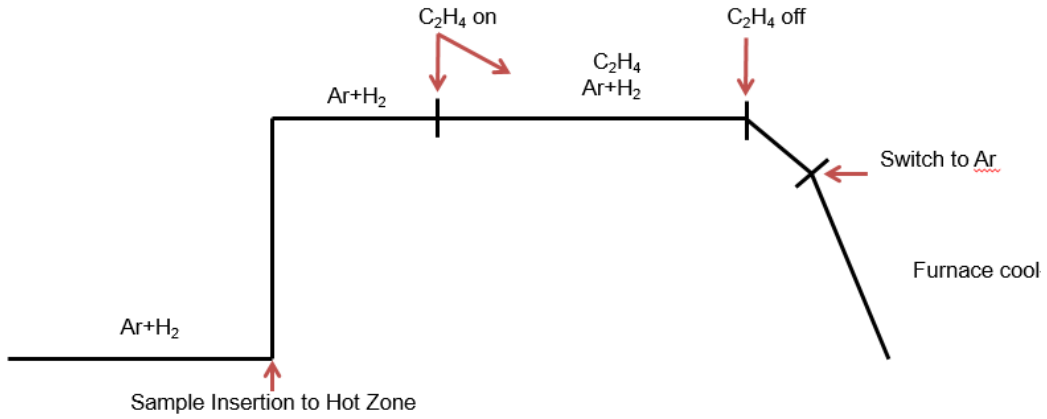


Figure 2-5: Reference CNT growth process

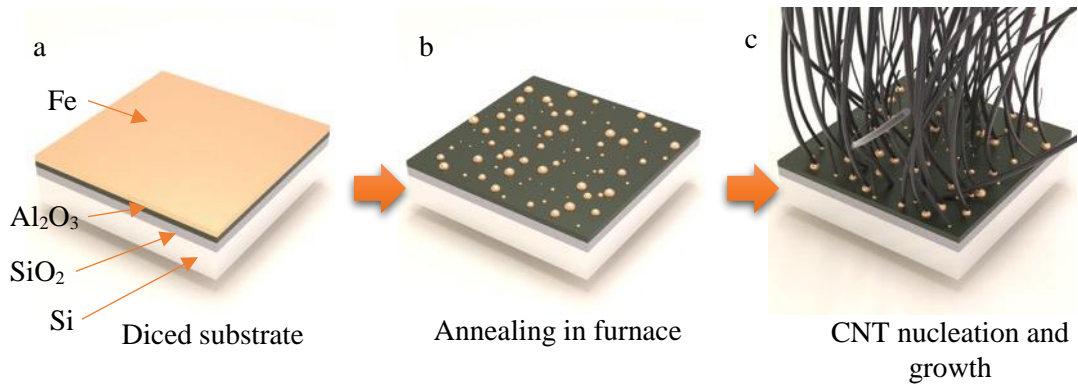


Figure 2-6: Catalyst layer annealing, and CNT nucleation and growth

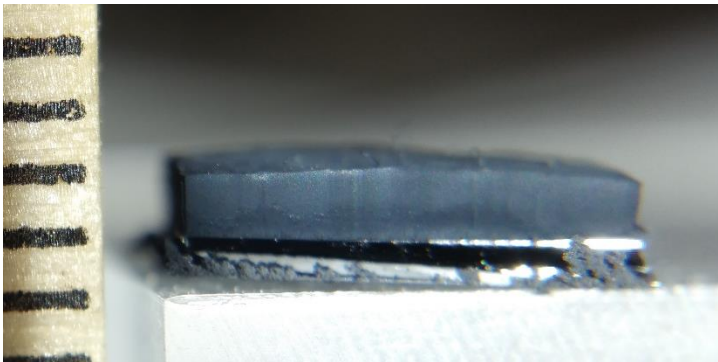


Figure 2-7: One millimeter long CNT forest grew on a 0.5×0.5cm wafer using our recipe.



Unfortunately, growing large quantities of CNTs, as required for this study, was highly time-consuming and may result in variations in CNT quality from one growth batch to another. We, therefore, used commercially available vertically aligned MWCNTs provided by GeneralNano, LCC. Structure and morphology of these nanotubes were investigated and are discussed in the next chapters.

### CHAPTER 3 : MANUFACTURING ALIGNED CNT STRUCTURES

Multiple groups have been able to align carbon nanotubes in the form of a 1-D fiber through dry and wet spinning techniques. In the solid-state method ('dry processing'), CNT fibers are spun directly from a CNT synthesis reaction zone or a pre-grown CNT array on a substrate. To our best knowledge, the highest reported electrical conductivity for these fibers is ( $1.71 \times 10^6$  S/m for Miralon yarn C-series);[98] for radially densified and doped fibers produced by the Nanocomp Technologies, Inc. The second approach ('wet processing') involves extruding a premade CNT solution/dispersion through a spinneret into a coagulation bath forming dense CNT fibers.[99] The highest reported conductivity for fibers made using this technique is reported by Rice University researchers.[100] A highly densified fiber made from a CNT/fuming chlorosulfonic acid solution and doped with iodine achieved a conductivity of  $8.5 \times 10^6$  S/m.[100] An 'ideal' CNT fiber would contain ultra-long, pure, defect-free, and small diameter CNTs that are densely packed and parallel to the fiber axis. These manufacturing techniques suffer from inherent processing limitations where they either cannot process long CNTs (wet processing) or produce fibers with poor CNT alignment and packing (dry processing). Despite a decade of R&D, these bottlenecks still exist and have limited the widespread production and utilization of these fibers for electrical wire applications. In terms of manufacturing, both wet and dry processing techniques are very mature, and other approaches are currently being sought to improve the properties of CNT fibers manufactured using these techniques. Some of these include densification,[101] CNT graphitization and purification using heat and current treatments,[102, 103] doping,[104-

106] synthesis of higher conductivity (metallic) nanotubes,[107] or selective elimination of lower conductivity (semiconducting) nanotubes,[108] and decoration of CNTs with gold, copper or silver nanoparticle.[109, 110] Although, all these approaches improve the conductivity of fibers, both wet and dry processing techniques fall short to achieve an ‘ideal’ CNT fiber and hence are not likely to result in fibers with conductivities higher than copper.

Tabulated in Table 1, are the best-achieved properties for bulk CNT fibers as well as conventional metals. When normalized by weight, bulk CNT fibers surpass the properties of best materials known to humans. CNT fibers have also achieved specific electrical and specific thermal conductivities (Conductivity/weight) in excess of copper properties.[99, 104, 109] Evident by the data in this table, there is a large room for improvement in CNT fibers.

Table 3-1: Density, electrical and thermal conductivities of best results for dry-process and wet-processed CNT fibers in comparison to individual CNTs, Copper, and Aluminum

Data in this table is provided for comparison purposes only.[111-113] Except for individual nanotubes, the highest achieved properties in each row correspond to different grades of each material.

	<i>Electrical conductivity</i> ( <i>S/m</i> ) $\times 10^6$	<i>Thermal conductivity</i> ( <i>W.m<sup>-1</sup>.K<sup>-1</sup></i> )	<i>Density</i> ( <i>g.cm<sup>-3</sup></i> )
<i>Individual CNT</i>	20-100	3000	1.4
<i>CNT fiber: dry processing</i>	<b>1.71</b>	<b>1230</b>	0.2-0.6
<i>CNT fiber: wet processing</i>	<b>8.5</b>	<b>635</b>	0.5-1.4
<i>Copper</i>	60	400	8.9
<i>Aluminum</i>	35	250	2.8

Other than CNT fibers, attempts have been made to produce CNT composite cables[114, 115]. The increase in durability and flexibility, as well as significant decrease

in overall weight, make CNT cables a promising alternative to current cables. Other CNT composite wires have been achieved by coating copper wires in CNT solutions by Holesinger et al.[7] Acid and water-based solutions have been used for CNT coatings. The

It's noteworthy that CNT structures have been grown directly on bulk objects such as copper wires using CVD methods.[116] This method offers some great advantages compared to its alternatives such as ease of processing. Although promising, not much research has been done in this field

### **3.1. Choice of CNT dispersion medium for CNTs**

Entanglement in CNTs during synthesis or purification processes [117] is the single major difficulty in making a true solution of carbon nanotubes. Surfactant-assisted ultra-sonication and dissolution in strong acids are the main methods for preparing CNT dispersions. Entangled CNTs go through an unzipping process with the aid of dispersants penetrating in their bundles and agglomerated and overcoming the nanotube-nanotube van der Waals attractions. Surfactants only act as stabilizers of nanotubes and require high energies to break apart nanotube agglomerates.[118] The energy is usually delivered by ultrasonication or shear mixing. These methods only aid in dispersing the CNTs and the surfactants are necessary to keep the nanotubes apart. Ultrasonication can be used to prepare individually dispersed CNT solutions. It, however, deteriorate nanotube structure during dispersion.[119] Polymers and organic solvents can also be used for CNT dispersion. While they have a minimal effect on the electronic properties of

nanotubes, their insulating nature has a great influence on properties of the resulting CNT fiber or wire and their removal requires additional steps.[13]

Using acids to prepare CNT dispersions is inherited from polymeric solutions used in processing of kevlar and other polymers. Acids have shown to be effective in eliminating van der Waals forces between nanotubes by protonation of the CNT sidewalls. Not only the type of acid used have shown to give different results in dispersing CNTs and altering their electrical properties, CNT characteristics such as number of walls, chirality, length and diameter have also shown to be influential in preparing the CNT dispersion.[120, 121] [122] Chlorosulfonic acid is a true solvent for CNTs.[123] Additionally, it's recently been shown that chlorosulfonic has a positive influence on electrical properties of CNT structures by reducing contact resistance between nanotubes.[124, 125] Chlorosulfonic acid can disperse higher concentrations of carbon nanotubes compared with alternative acids. It is noteworthy that at higher concentrations, biphasic solution and eventually, formation of liquid crystal boundaries in adjacent boundary grains have been observed in CNT-acid solutions. This can be utilized to facilitate alignment and densification in CNT fibers.[126]

Sulfuric and Oleum also result in high levels of nanotube dispersion by protonation.[127] However, their effect on the electrical properties of CNT remains questionable. Some research shows that they may generate defects on the CNT sidewalls, though there are arguments that functionalized groups can be beneficial for electrical properties.[122, 128] Moreover, nanotubes can be dispersed at much higher concentrations in acids than other solutions. A critical consideration when preparing CNT solutions for wet processing is the rheology and viscosity of the resulting solution.

Generally, CNT concentration and viscosity need to be higher than a threshold limit for effective alignment. Additionally, longer nanotubes in a structure resulting in a lower number of junctions, thus a higher conductivity. On the other hand, lower concentrations can be achieved for a solution with longer CNTs; similar to dispersions of polymeric rigid rods.[118] Ultra-long single-walled CNT (SWCNT) are not dispersable in sulfuric acid.[129] Another note on CNT dispersions with sulfuric acid is that by introducing small amounts of water in the solution, aligned bundles of CNTs can be formed.[118] It is also predicted that this bundle size has a direct correlation with fiber's conductivity.[13]

### **3.2. Other parameters affecting CNT dispersions**

Efficient electrical/thermal transport requires metallic nanotubes (carbon nanotubes are usually comprised of both semiconducting and metallic nanotubes). As such, the highest electrical conduction in pure CNT wires ( $10^8$  S/m) is predicted for metallic (defect-free: zero band gap), ultra-long, and single wall nanotubes.[130] However, industrially relevant bulk quantities of high-quality metallic CNTs cannot be currently synthesized,[107] and available methods to separate CNTs based on their metallic/semiconducting nature are only applicable to microns long CNTs and have a very low yield. Dopants have, however, been successful in decreasing the band gap in semiconducting nanotubes by charge transfer. For example,  $\text{KAuBr}_4$ , [101] iodine monochloride (ICl), [105] and iron chloride ( $\text{FeCl}_3$ ) [106] have significantly enhanced electrical transport in carbon nanotube and graphene structures, respectively. The stability of dopants at high temperature remains a concern. Alternatively, semiconducting CNTs

can be selectively etched, for example using hydrogen peroxide [108] or sulfur trioxide (SO<sub>3</sub>).[131] Recent lab scale demonstrations have also shown the potential of a nanocomposite approach (aligned single-walled CNTs and copper) to outperform copper in electrical conductivity above 80 °C.[109]

Although individual carbon nanotubes can have electrical conductivities of up to  $1 \times 10^8$  S/m in the case of SWCNTs and  $3 \times 10^6$  S/m for MWCNT, as the highest conductivity for a CNT fiber, to date, is  $8.5 \times 10^6$  S/m.[100] Recent research by Zhao et al. have shown that Iodine doped CNT fibers had an electrical conductivity of  $6.7 \times 10^6$  S/m ( $1.5 \times 10^{-7}$  Ω.m) which is approximately tenfold lower than copper ( $5.96 \times 10^7$  S/m).[104] Other than doping, the contact resistance between individual CNTs in the fiber, twist and length of CNTs, their alignment, packing density and entanglements also affect electrical conductivity in CNT fibers.

Impurities can adversely affect properties in macroscale CNT conductors.[111] That is either by acting as scattering sites for electrons or hampering packing and alignment during CNT fiber fabrication. Furthermore, the CNT-CNT junction resistances dominate transport in CNT assemblies. Increasing individual CNT length and chemical doping has shown to decrease this contact resistance.[99, 132, 133] To address these two issues, the wet processing method studied in this thesis, utilizes highly pure and millimeters long CNTs, therefore significantly reducing the number of junctions. The length of nanotubes that can be processed with this method is only limited by the current ability to grow nanotubes, i.e., up to ~1 cm.[134, 135] In this method, we use high purity but low quality vertically aligned CNT (VACNT) arrays grown via CVD. These CNTs are detached from the substrate (leaving almost all catalyst particles behind) and

subsequently dispersed in diluted sulfuric acid, forming fibers. This is due to the CNTs' pre-alignment, millimeters length, high rigidity and large diameter of the fiber (up to hundreds of microns). Formation of CNT fiber structures facilitates packing and alignment during subsequent processes of solution coating and wire drawing. Both the wet and dry fiber manufacturing techniques described earlier pose serious limitations to obtaining an 'ideal' CNT fiber. Dry processed fibers contain impurities (catalyst particles and amorphous carbon) that significantly degrade their performance and suffer a low packing density and poor nanotube alignment inherent to the spinning process.[111, 112] CNT end junctions limit the electrical performance in fibers;[99, 136] hence much effort has been focused on growing longer CNTs to reduce the number of junctions per length in CNT fibers. Wet-processed fibers, on the other hand, are comprised of dense, highly aligned, and pure nanotubes.[99, 104] Unfortunately, only microns long nanotubes can be processed using the existing wet processing extrusion methods.[137]

In order to address the shortcomings of the existing aligned CNT structure technique, we examined a new process that enables aligning millimeters long nanotubes. In this process, CNTs are detached from the substrate and subsequently dispersed in 98% sulfuric acid (short single or few-walled carbon nanotubes may also be added to the solution at this stage) forming CNT fibers as shown in Figure 3-1 (i.e., semi-rigid bundles of nanotubes), then a nylon or copper wire was dip-coated with the CNT fibers. The CNT coating on the wire is progressively wire drawn to form a highly packed and aligned CNT coating. The pre-alignment and long lengths of the VACNTs used in this technique facilitate their assembly by solution coating and wire drawing into a packed and highly aligned structure. This method utilizes capillary and mechanical forces to align and



densify a thick CNT coating. The wires were dried for a minimum of 12 hours in ambient temperature, their electrical conductivity is measured, and their structures were studied with the aid of scanning electron microscopy (SEM) and Raman Spectroscopy techniques. Other than the application for wiring, this method can be conformed to electromagnetic shielding of cables, thin film antennas, and composite electrodes with CNT structures.

In summary, the proposed wire fabrication method may offer the following key advantages:

- Depending on the application, various substrate wires may be used. For electrical applications, copper or aluminum wires are a natural choice, whereas, for structural applications, polymer fibers may be used.
- Controlling wire diameter in both wet and dry processing methods is complicated, and they usually produce fibers that are tens of microns in diameter. The proposed method allows for manufacturing different wire diameters (up to millimeters) by changing the diameter of the substrate wire and/or coating and processing parameters.
- Upon acid dispersion, CNT arrays maintain their alignment and collapse to form fibers (rather than entangled CNT bundles). This facilitates alignment and packing of coatings during solution coating and wire drying processes.
- Solution coating and wire drawing are both low-cost, high-rate and highly scalable. Wet chemistry processing of CNTs resolves environmental and toxicological concerns with suspended CNT particulate matter of respirable size.

- The copper core will allow for conventional soldering and insulating coatings to be used for connections and insulation, respectively.

The set of experiments designed for this study were developed after numerous trials carried out using various solutions and processing parameters. Endeavors on electrical conductivity measurements of these coatings shed light on the importance of the adhesion of the CNTs to the substrate.

### **3.3. Experimental**

#### *CNT solution preparation*

Vertically aligned multiwall CNTs (MWCNT), 1-2mm in height and a Raman G to D peak ratio of  $\sim 1.6$ , were acquired from General Nano LCC. Tuball<sup>TM</sup> SWCNTs were obtained from OCSiAl. According to the manufacturer, the SWCNTs are longer than  $5\mu\text{m}$ , contain more than 75% nanotubes and exhibit a Raman G to D peak ratio of  $\sim 50$ . Both nanotubes were used without further processing. MWCNTs and SWCNTs were dispersed in industrial grade sulfuric acid in small batches by means of magnetic stirring for 1-2 h. Stirring with magnetic stirrer avoids any damage to CNTs in the solution. Each batch consisted of 50mg of CNTs in 100ml Sulfuric acid. Two main solutions were made from the small CNT batches. We tried coating copper and nylon wires from solutions of both short (a couple of microns) and long (few hundreds of microns) SWCNTs in sulfuric acid. Neither solution was able to adhere to the substrate wire and coat it. The main component for coating formation was, therefore, identified to be the long MWCNTs. As such, shearing of the MWCNT forests breaks them into fibers that are tens to hundreds of microns in diameter and as tall as the pristine CNT forest (Figure 3-1).

In this study, we'll try to gain a better understanding of the influence of SWCNTs on the structure and performance of conductive CNT coatings alongside the general performance of the wires achieved using the coating/wire-drawing approach. Two main solutions were used, solution #1 consisted of 250mg MWCNTs in 400ml sulfuric acid and solution #2 contained 125mg MWCNT and 125mg SWCNT in 400ml sulfuric acid (0.0232 wt.% CNTs). SWCNTs were used to fill in the voids between the ultra-long MWCNTs. 100ml of DI water was slowly added to both solutions for aiding the formation of larger aligned bundles and lowering the viscosity of the solutions for easier stirring. Figure 3-1 shows the dispersion of the carbon nanotubes in the solution by forming nanotube bundles. The bundles are formed due to the large van der Waals forces between individual CNTs, entanglements, and friction forces. Solutions were mechanically stirred at 200-400 rpm in a 500ml beaker during the dip-coating process.

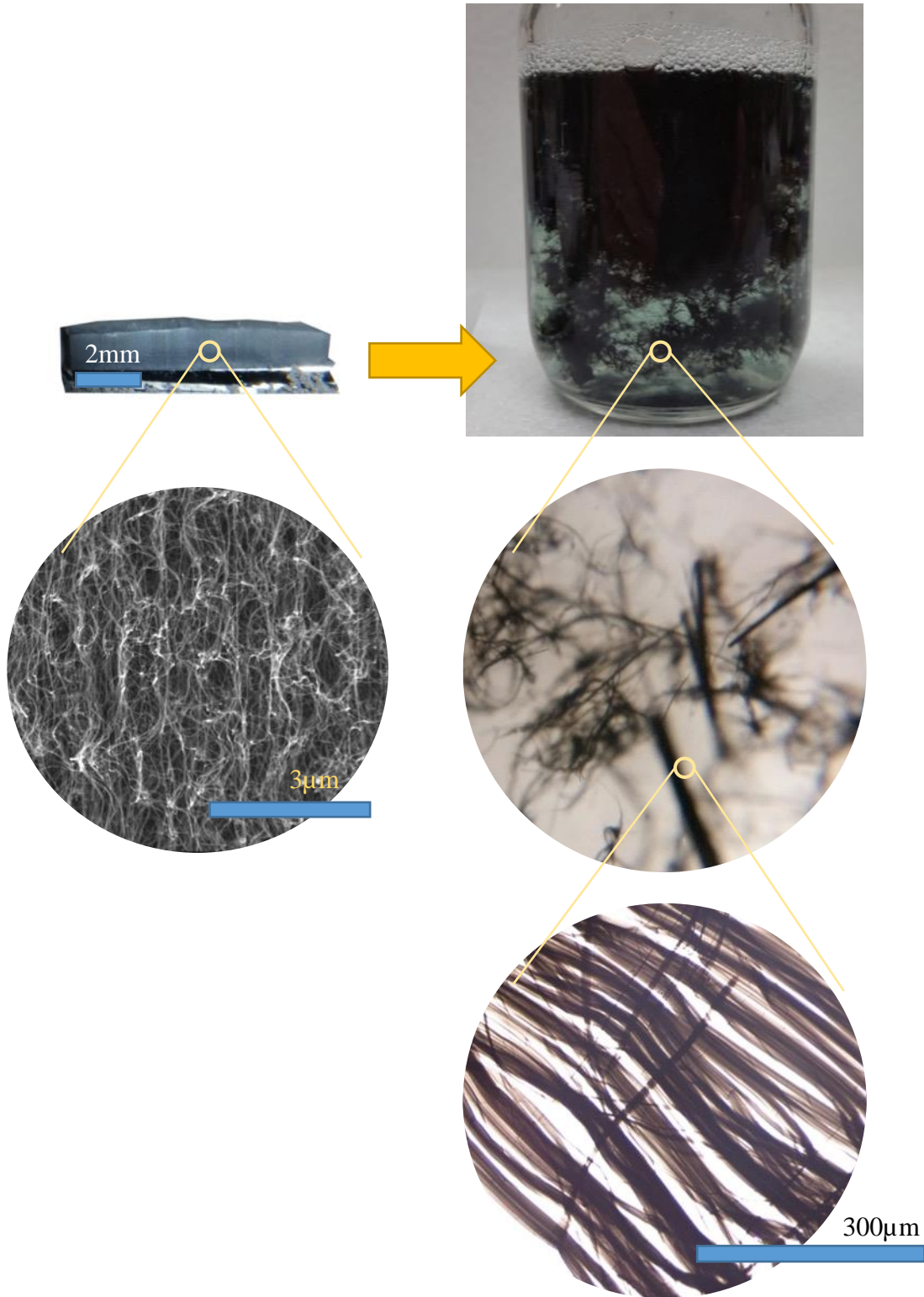


Figure 3-1: 2mm long MWCNT forest dispersed in 98% sulfuric acid with the aid of mechanical stirring, forming micron-size MWNT bundles.

### *Dip-coating process*

Dip-coating of both copper and nylon wires from solutions of both short (a couple of microns) and long (few hundreds of microns) SWCNTs in sulfuric acid was examined. Neither solution was able to adhere to the substrate wire and coat it. The main component for coating formation was, therefore, identified to be the long MWCNTs. As such, shearing of the MWCNT forests breaks them into fibers that are tens to hundreds of microns in diameter and as long as the precursor CNT forest, as shown in Figure 3-1.

Copper wires, 24 American wire gauge (AWG) or 511 $\mu$ m in diameter, were abraded with 240 grit sandpaper for better adhesion to CNTs. These filaments, cut in 10 cm long pieces, cleaned in an ethanol container inside a sonication bath and dried by nitrogen flow. Prepared copper wire substrates are dipped into the solutions and extracted to form the CNT coating.

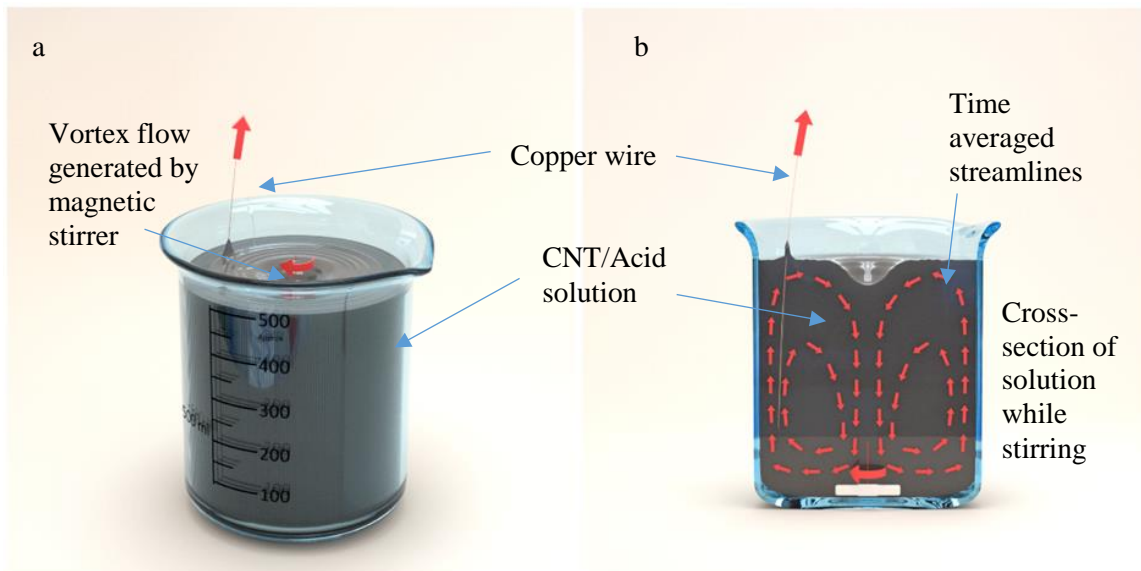


Figure 3-2: Left: Schematic for the dip-coating step of a copper wire in stirred solution. Right: Cross-section view of the dip-coating step with streamlines generated in the solution resulted from stirring.

In addition to copper, nylon was also used as a substrate for CNT coating. This was to exhibit the versatility of the coating technique and also due to the insulating nature of nylon that facilitated direct measurement of the electrical conductivity of the coating.

For lighter nylon monofilament wires, dip-coating is difficult as the wire meanders in the solution upon entering it. To overcome these issues and convert the simple dip-coating to a continuous coating process, wires were passed through a thin glass straw to the bottom of the solution and extracted from the bottom side of the straw in the upward direction of streamlines with a slight angle in the direction of vortex flow to form ~20 cm long CNT coated sections for this study (Figure 3-3).

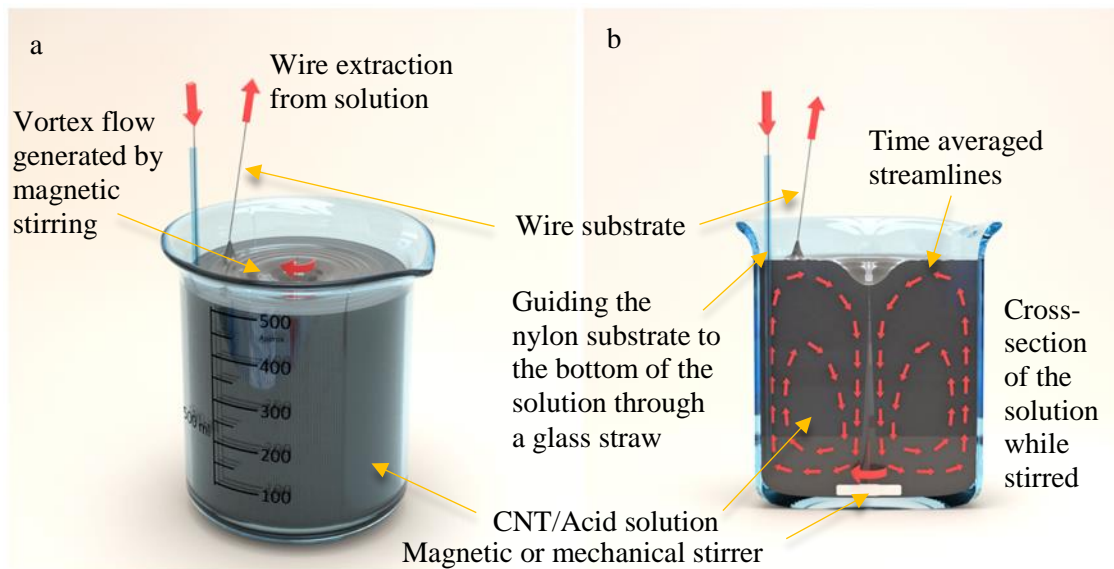


Figure 3-3: a) Schematic of CNT solution dip-coating process of Nylon wires. b) A cross-sectional view of the solution with streamlines generated in the solution while stirring.

Vortex flow patterns generated by a magnetic propeller in a glass cylinder were described by Halasz et al. [138] As shown schematically in Figure 3-2 and Figure 3-3, the three-dimensional flow patterns can be exploited to form more uniform and unidirectional CNT structures on substrate wires. In this regard, CNT structures can be considered as polymeric rods in a solution, [118, 139] and thus will track the streamlines. Aligning the wire with these streamlines can, therefore, result in the formation of aligned CNT coatings. The container shape can affect the vortex flow generated in the solution by mechanical stirring. By adding the thin straw to the inner sidewall of the container, continuous coating was achieved by guiding the wire to the bottom of the container and extracting it from the solution with minimum influence on the vortex flow (Figure 3-3).

All coated wires were rinsed in DI water after the dip-coating step. Half of the wires at this point were hung under the fume hood to dry overnight. The second half of the wires went through the die drawing process starting with 2.2mm diameter die and ending with 460 $\mu$ m and 550 $\mu$ m diameter dies for nylon and copper wires, respectively, in 12-19 drawing steps (Figure 3-5). DI water rinsing was employed, as needed, in-between each drawing step of the process for lubrication. In the case of nylon coated wires, immediate immersion in DI water after the dip-coating process is necessary to remove the excess sulfuric acid that would otherwise deteriorate the nylon core and eventually (in a matter of minutes) result in the breakage of the nylon core.



Figure 3-4: CNT coated samples with nylon core

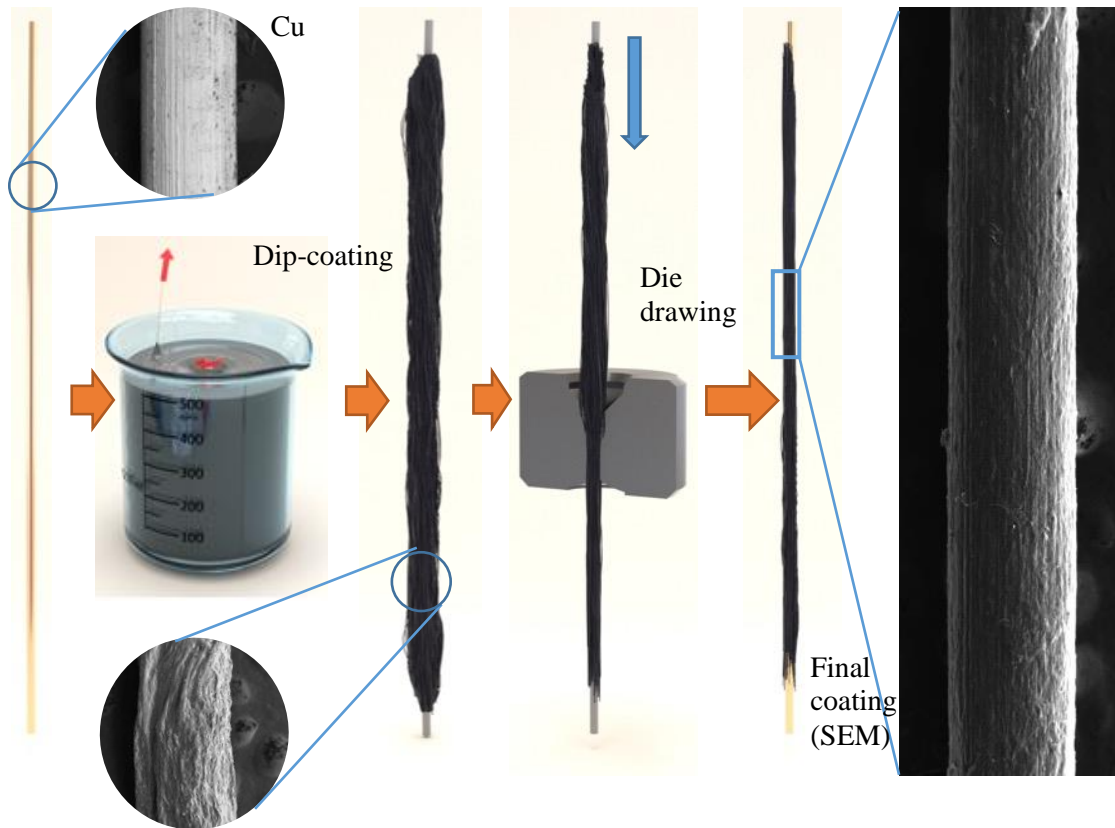


Figure 3-5: Schematic of the coating process of wires with dip-coating and densification of the coating in die drawing steps. SEM images of the substrate and coating are included to complement the schematics.



### *CNT coating / substrate interaction*

Surface characteristics of the substrate wire affect the CNT coating quality and thickness. In order to improve adhesion of CNTs to the substrate and promote coating, several surface treatments were examined. Some surface treatments prohibited the formation of any coating while others resulted in uniform and thick ones.

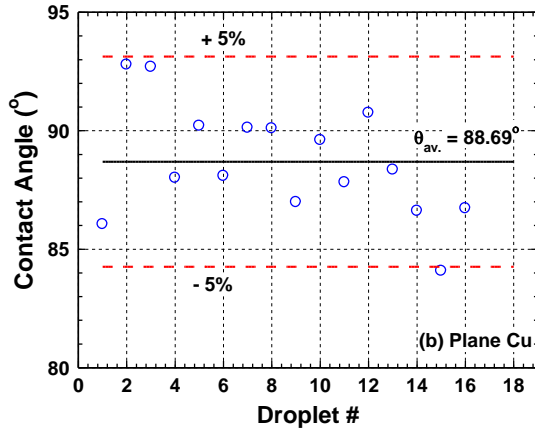
Contact angle measurements of water droplets on copper foils, with different surface preparations, were carried out to understand the coating process better.

Contact angle measurements were performed based on ASTM standard D7334-08 with a ramē-hart static contact angle goniometer. Deionized water droplets with volumes less than 20 $\mu$ L were used in these measurements. The ASTM standard recommends the measuring time for each droplet after hitting the surface not to exceed 30 seconds. The average contact angles were measured for 10-20 droplets for each sample. Measurements were taken place on untreated and treated copper tape. Treatments included abrading with 240grit sandpaper, 400grit sandpaper, hydrochloric acid, and nitric acid. Data variations recorded for contact angles are 5 to 6%.

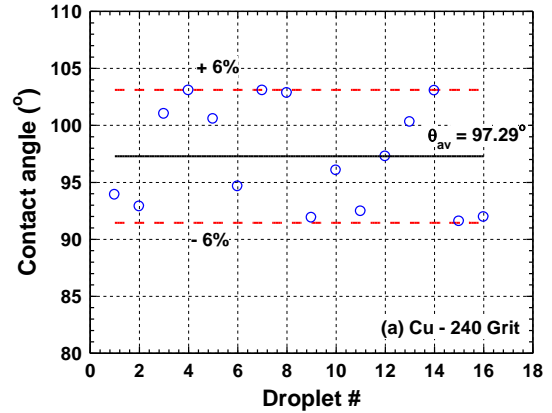
Acid treatment and surface roughening were used to oxidize the surface and increase the surface area, respectively, resulting in contact angles between 65 and 100 degrees. The copper surface roughened by a 240 grit sandpaper exhibited the highest contact angle, or a higher hydrophobicity, while nitric acid treatment resulted in the most hydrophilic surface among the tested surfaces. Copper substrate wires with identical surface treatments were prepared, and it was observed that the coating uniformity increases with contact angle values of the surface. No coating was formed on the wires treated with nitric acid, and the most uniform one was formed on the wire sanded with the 240 grit

paper. Coating formation is therefore governed by the surface hydrophobicity, in that, a more hydrophobic surface will repel the acid more, and CNTs can better adhere to it, whereas CNTs do not attach to the surface if it is hydrophilic. This is especially true if the coating is formed at the interface of the air/solution where it can stay on the substrate if the substrate surface rids of acid, i.e. if it is more hydrophobic. The 240 grit sandpaper roughening was used to modify all the copper substrate wires used in this study. The increased surface area of the wires due to this treatment also enhances the contact area between the coating and substrate.

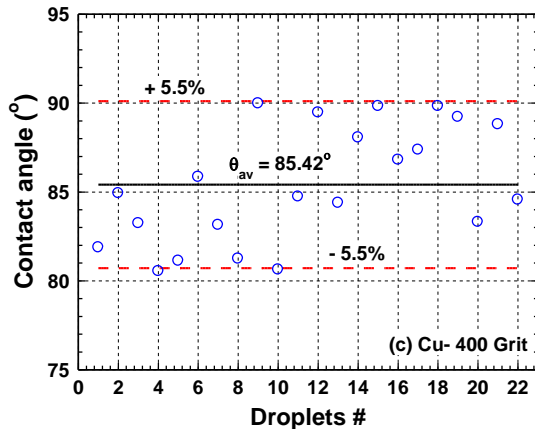
Untreated



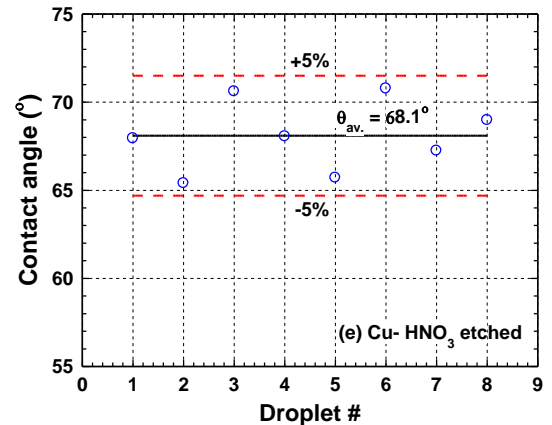
240 Grit



400 Grit



HNO<sub>3</sub>



HCl

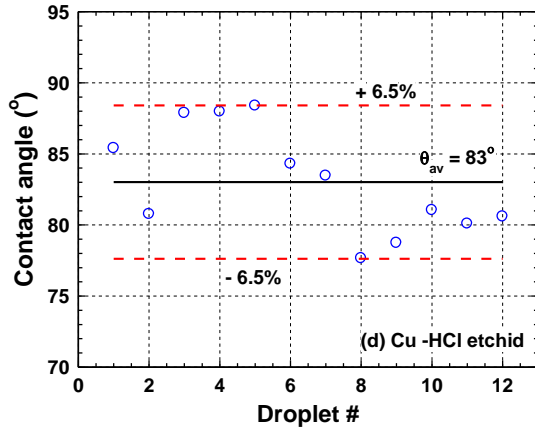


Figure 3-6: Contact angle measurements of water droplets on copper tape, untreated, and treated with 240grit sandpaper, 400grit sandpaper, Nitric acid, and Hydrochloric acid.

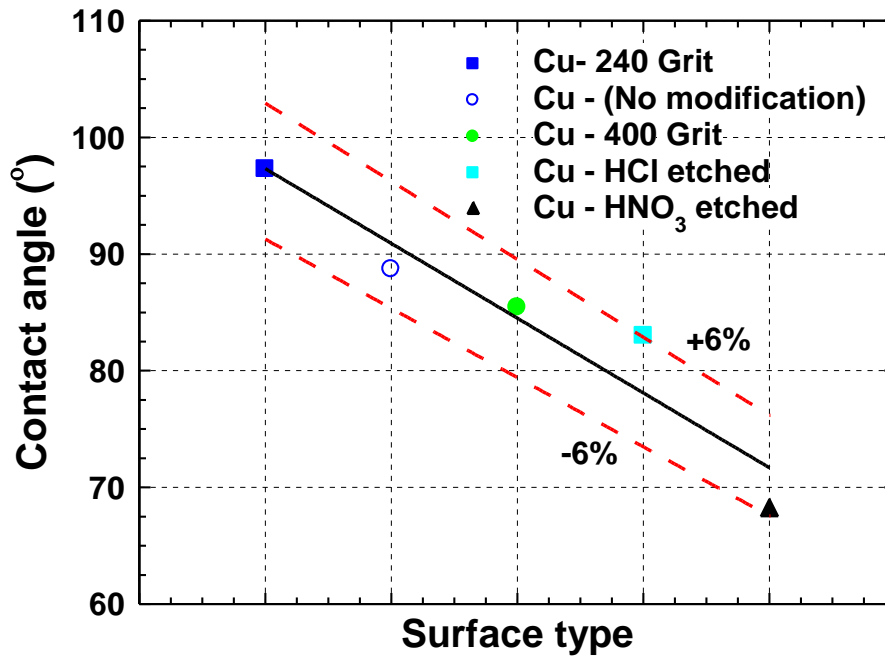


Figure 3-7: Summary of contact angle measurements of water droplets on copper tape, untreated, and treated with 240grit sandpaper, 400grit sandpaper, Nitric acid, and Hydrochloric acid.

A simple test has been carried out for visual adhesion test of the prepared samples with an applying pressure with an adhesive tape on the coated section of the wire and removing it (Figure 3-8).

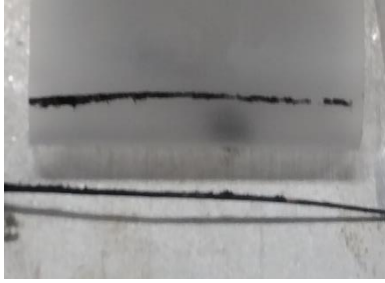


Figure 3-8: Simple CNT coating adhesion test on a CNT coated copper substrate with adhesive tape.

In addition to copper, nylon was also used as a substrate for CNT coating. This was to exhibit the versatility of the coating technique and also facilitate the direct measurement of the electrical conductivity of the coatings. Similar to copper, CNT fibers adhere well to nylon. Nylon, however, was slightly corroded (or etched) upon exposure to sulfuric acid. This corroded surface layer acted as a hospitable porous structure for CNT adhesion. As shown in Figure 3-9, the bright layer between the nylon core and CNT coating is a porous structure consisting of nylon and CNTs. To confirm that this layer is formed in the process, a nylon wire was dipped in and retracted from a CNT free sulfuric acid in the same manner as the coating process. Comparing cross-sectional microscopy pictures taken from this sample (Figure 3-9b) to un-treated nylon wire shows the formation of this corroded layer on nylon filaments.

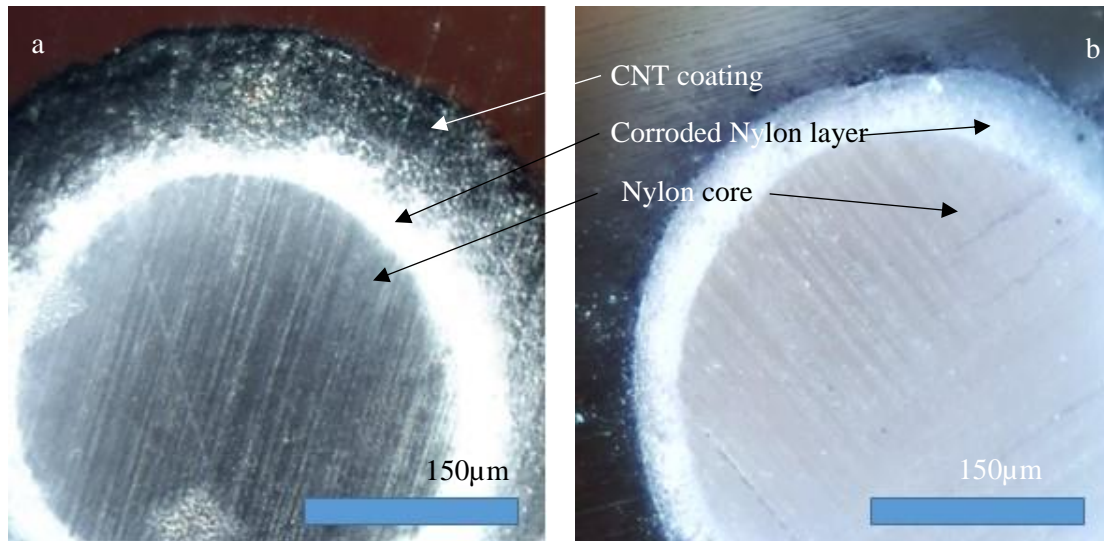


Figure 3-9: Cross-sectional dark field microscopy images of CNT coated nylon wire (a), and sulfuric acid treated nylon wire (b).

Different processing parameters affect the CNT coating quality and thickness. For example, die drawing can be used to densify the coating on a substrate wire, uniform it, and coax CNT fibers to align in the wire direction. Moreover, it was found that stirring rate of the CNT-acid solution has a prominent influence on the formation and uniformity of coatings. Specifically, no coating was formed at both relatively low and high shear mixing rates, respectively. To monitor the effect of die drawing and shear mixing rate on coating uniformity, alignment, and packing, several samples under different processing conditions were prepared. One group of wires were drawn through a series of dies after dip coating, and another group was simply dried after dip coating. Similarly, samples from each solution were prepared under different shear mixing rates, half of which at rates close to the lower limit of coating formation, and the other half close to the upper limit for coating formation. Finally, samples based on ultra-long MWCNTs and a mixture of both ultra-long MWCNTs and short SWCNTs were prepared. SWCNTs were used as

a filler to occupy the spaces between the long nanotubes. The summary of the wires prepared in these experiments are provided in Table 3-2. Structure and properties of samples in each group was then investigated in order to elucidate the effects of processing, namely die drawing and shear mixing rate, thereby closing the processing-structure-property relationships loop.

Table 3-2: Summary of the samples prepared for this study. 16 Samples (Average coating length of 15 cm per sample)

	<i>MWCNT solution</i>		<i>MWCNT/SWCNT solution</i>	
	High shear rate	Low shear rate	High shear rate	Low shear rate
<i>Nylon core</i>	Die drawn	x	x	x
	Not die drawn	x	x	x
<i>Copper core</i>	Die drawn	x	x	x
	Not die drawn	x	x	x

## CHAPTER 4 : ELECTRICAL CHARACTERIZATION OF WIRES AND COATINGS

### 4.1. Wire diameter measurements

A laser micrometer (XACTUM XLS 13XY) with custom-made sample mount (Figure 4-1) platform was used for measuring the diameters of the composite wires and the copper cores. Measurements were taken in 1mm increments along the coating and core length. The average diameter was then employed to calculate the cross-sectional area of the wires and their coatings. The standard deviation of these measurements was used later for the uncertainty analysis of the results.



Figure 4-1: Laser micrometer setup with custom-made sample holder for measuring the diameter of Nylon and Copper wire substrates as well as CNT coated composite wires

Prior and after dip-coating the wires into the solution, initial and final weights of the wires were measured. The difference was considered to be the weight of the coating, and the density of the coating was accordingly calculated.

Figure 4-2 shows the coating thickness, coating area, and coating's surface variations for the wires formed on nylon and copper and subjected to die drawing. It can be concluded from this figure that on average, thicker coatings are formed on nylon than copper substrates, which indicates the higher adhesion levels for CNTs to the nylon. It is also observed that die drawing has a more prominent effect on both the densification and surface roughness of the CNT coatings in CNT-copper wires compared with coatings on nylon wires. On average, CNT coatings on nylon are smoother regardless of whether they have been through the die drawing process or not.

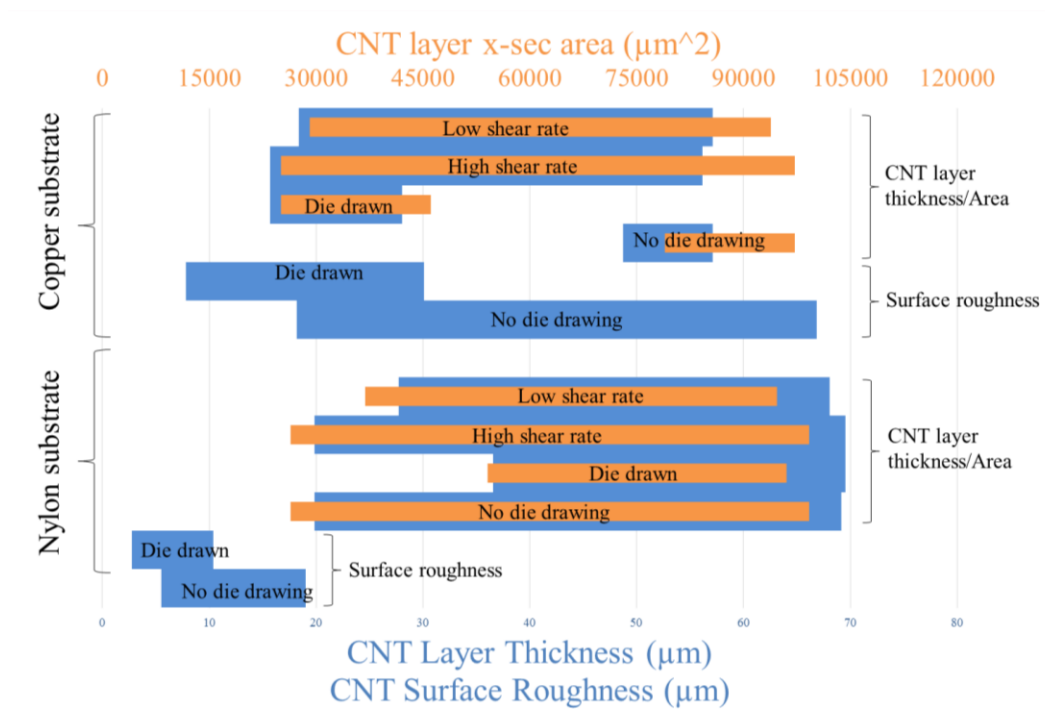


Figure 4-2: Coating thickness range achieved for the composite wires (nylon and copper as substrates), coated at different shear mixing rates and subjected to die drawing. Average surface roughness of as coated and wire-drawn CNT coatings on copper and nylon substrates are also included.



## 4.2. Electrical Conductivity measurements at room temperature

The resistance of the wires were calculated using the Ohm's law, e.g., by applying a known current and measuring the resulting voltage. For high conductivity materials, measured voltage is very small, and various sources of errors and noises occur as a result.

In a simple two wire DC method using a multimeter, a current is passed through the sample, and the resulting voltage is measured across the terminals. The resistance is calculated by dividing this voltage by the current. This method is not accurate for resistances less than  $100\Omega$ . It's noteworthy that the drop in voltage is due to the device's resistance as well as leads' resistances and connections.

An alternative method is a four-probe connection which eliminates the lead resistances from measurement. In this method, DC passes through the specimen and the voltage is measured with separate leads.

Although this method is suitable for resistance measurements under  $100\Omega$ , there are still other sources of errors and noises for low resistance measurements. The most common source of measurement errors for electrical conductivity is thermoelectric voltages that develop in response to temperature gradients, or when dissimilar materials are touching. Avoiding the employment of non-copper leads can terminate the latter source of error. Also, keeping the setup on for prolonged periods of time before starting the experiments and placing all the components as close as possible can cause the setup to reach to a temperature equilibrium with the surrounding environment which minimizes the former. Another highly effective method is to use a reversing current source to cancel

thermoelectric EMFs. Averaging the measurements between two reversed readings results in canceling the Thermoelectric EMFs from calculations.

$$V_1 = V_{emf} + V_a - V_b$$

$$V_2 = V_{emf} + V_b - V_a$$

$$\frac{V_1 - V_2}{2} = V_a - V_b$$

Another source of error is non-ohmic contacts which may result from oxidations as an example, and there are various ways to check for them which we are not going through here.

Without the consideration of noises in a typical two-probe measurement system for a device with resistances, less than  $10\text{m}\Omega$  which is the range of our measurements, the errors due to lead resistance, connection resistance, and terminals can cumulate to values greater than the true resistance itself.

Other than these measurement errors, there are several sources of noise which influence low resistance measurements. All voltage sources generate Johnson noise due to their internal resistance, and it can be reduced by decreasing the bandwidth of the measurement and the temperature of the setup which are not always options for experiments.  $1/f$  noise is another noise which is caused by environmental factors and chemical processes in the test components.

As mentioned before, the current reversal method can compensate for thermoelectric EMFs generated in the measurement. The delta mode is similar to current reversal method, but it uses three voltage measurements instead of two for every calculation by each polarity change. The additional term in averaging results in

eliminating thermoelectric voltages, thermoelectric voltage changes, as well as lowering noise levels.

One more consideration which is device heating should be accounted for low resistance measurements. The resistance of the device can change due to the power dissipation from the current source. This power can be calculated from the  $P = RI^2$  formula. This formula shows that using lower currents can decrease this effect.

The temperature changes in a sample for each measurement can be calculated from the following formulas:

$$I.V.t = M.C_p.\Delta T$$

$$M = L.\rho.A$$

Which I, the measurement current, V, the measurement voltage, M, the total weight of the portion of the sample under test,  $\rho$ , the density of the sample, A, the total averaged cross-section of the sample, and L, the length of the sample under test are measured in experiments and by assuming  $C_p=0.75$ , the heat capacity of graphite, we can obtain the temperature change of the sample during each process which usually takes between 5-10 seconds. Based on these rough calculations, the four-probe DC sweep method generates a temperature change of about 1°K and less in the sample during each measurement, and the Delta method generates temperature changes in the order of milli-Kelvins. These numbers do not hold true for conductivity measurements of the samples with plastic core, and they show higher power dissipations across the sample for each test even with low currents which results in temperature changes in the order of tens of degrees Kelvin.

The four probe delta mode was used for measuring the electrical conductivity of the wires at room temperature. A custom made four probe apparatus with copper connections and silver paste contacts were used. ASTM standard B193-16 and D4496-13 were followed. Conformity for the length of samples under measurements could not be achieved due to the short lengths of coatings compared to the lengths specified in ASTM standard B193-16 (300mm). The current was supplied by a Keithley 6221 DC/AC Current Source and voltage drops across the samples were measured by a Keithley 2182A Nanovoltmeter. The setup was controlled by a computer via LabVIEW. Resistance measurements were performed for 10mm long sections (distance between the voltage probes), from coated sections of the CNT coated wires, substrate copper core, and removed CNT coatings from copper substrates. Contacts to the specimens were made by carefully applying silver paste with the tip of a syringe. The applied current in the four probe delta mode was  $\pm 20 \times 10^{-6}$  Amps.

Four-probe electrical conductivity measurements of the CNT coated nylon wires, and the separated coatings from the copper substrate wires were performed by connecting the voltage probes on either the top or bottom side of the wire and placing the current probes on the opposite side. Results from these configurations were consistent with the results where all probes were placed on only one side of the wire, showing a uniform flow of electrons around the circumference of the wires in the 1 cm distance between the voltage probes. The linear dependence of voltage and current were also confirmed using the four probe DC sweep conductivity measurement. The electrical conductivity of the CNT coated copper wires were measured in three steps. First, the diameter of the composite wire was measured along the coated section as well as the resistance of the

coated section. Second, the wire was soaked in DI water and coating was removed with care; this process couldn't be applied to the coatings on nylon as there is a much stronger interaction between the coating and nylon in these samples. And lastly, the diameter of the copper core which previously was under the CNT coating was measured along the wire and resistance of that section was also measured. Another method with a higher success rate for separating the CNT coating from the copper substrate was to soak the wire in nitric acid instead of water. Nitric acid readily dissolves copper, and the coating can thus be removed. The two methods resulted in similar conductivities for the removed CNT coatings.

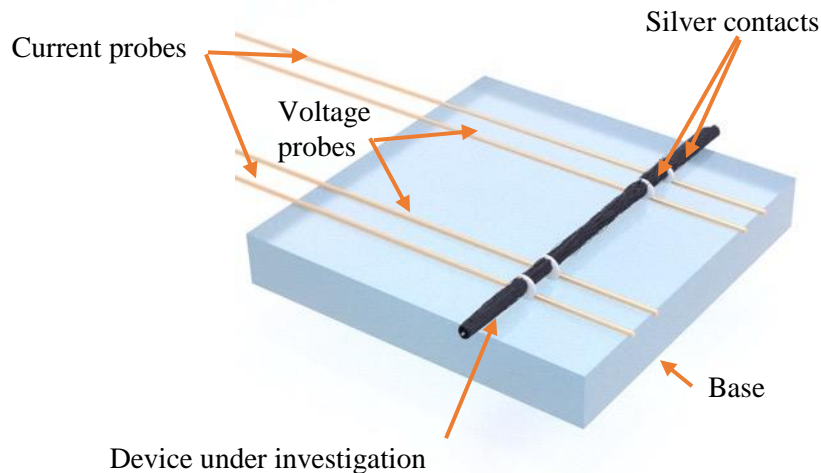


Figure 4-3: Experimental setup for electrical resistivity measurement: (a) top view; (b) isometric view.

To better understand the connectivity of the coating to the copper core, parallel resistance rule, as shown in Figure 4-4 was applied. This model calculates the

conductivity of the coating based on the two values of composite's conductivity and core's conductivity from the following equations:

$$\frac{1}{R_{comp.}} = \frac{1}{R_{Cu}} + \frac{1}{R_{CNT}} \quad (1)$$

$$\sigma_{CNT} = \frac{A_{comp.} * \rho_{Cu} - A_{Cu} * \rho_{comp.}}{(A_{comp.} - A_{Cu}) * \rho_{comp.} * \rho_{Cu}} \quad (2)$$

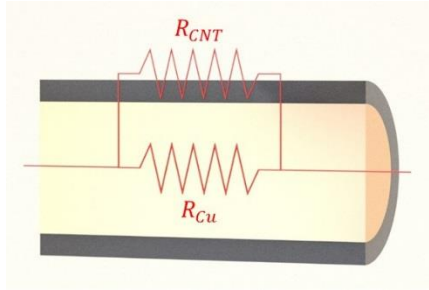


Figure 4-4: Parallel resistance model for the copper-coated wires. This model assumes an infinite resistance at the copper-coating interface.

In these formulas “R” refers to the wire resistance, “A” is cross-sectional area of the sections measured by laser micrometer, “ρ” is the resistivity of the sections and “σ” is conductivity. The subscript of “comp.” refers to the total copper-CNT coated composite wire, “CNT” is the carbon nanotube coating and “Cu” refers to the copper core. The conductivity of the CNT coating was measured separately after separation from the copper core and calculated using the previously known values using equation 3.

$$\sigma_{CNT} = \frac{l}{R_{CNT}(A_{comp.} - A_{Cu})} \quad (3)$$

In this formula, “l” is the distance between current probes in the four probe measurement apparatus. The coating conductivities calculated from equation 3 and direct

measurements do not match, which explains that: 1) CNT coating and copper core are not parallel resistors, and 2) there is a contact resistance between CNT coating and copper core. On the other hand, results calculated directly from equation (3) are in good agreement with the conductivities measured from CNT-nylon core wires. The highest conductivity achieved for the CNT layer in this study was 545.7S/cm. An increase of 46.8% in the average conductivity of all samples was observed in the samples from MWCNT/SWCNT solution compared to the samples from MWCNT solutions. This increase was due to the high quality of the SWCNTs and that they filled in the voids between the longer MWCNTs.

An interesting phenomenon observed for the CNT coatings removed from copper cores was the overflow of voltage at around  $5.2 \times 10^{-3}$  -  $6.1 \times 10^{-3}$  Amp current in the four probe setup, which was reversible, and at this point, we have no explanation for it (Figure 4-5). Also, an exponential decrease in resistance of CNT coatings was observed through the first 20-30 minutes of continuous measurements in the four probe delta mode electrical conductivity measurement (Figure 4-6). Figure 4-7 shows our results in comparison with the best results published for conductive CNT fibers and wires in literature to date, in terms of conductivity and cross-sectional area of the CNT portion of the wires.

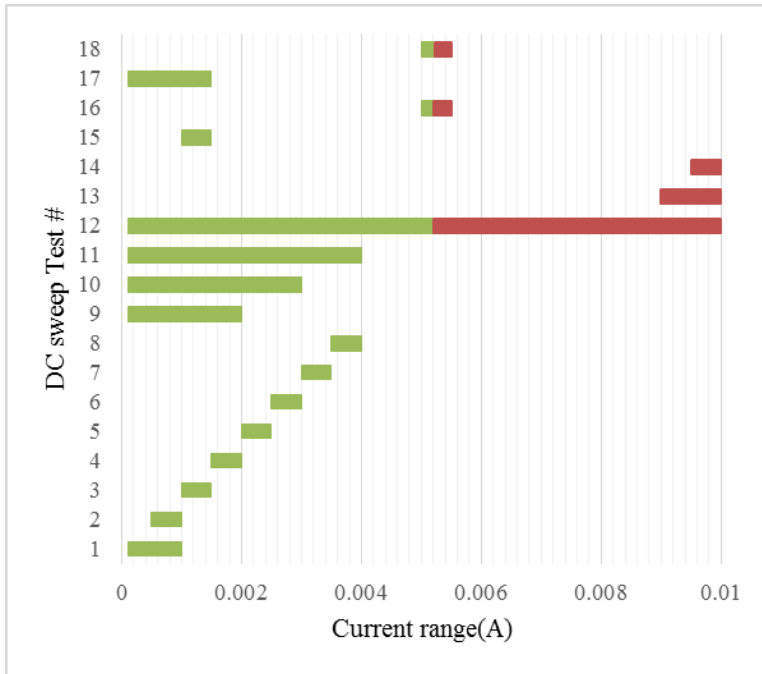


Figure 4-5: Four probe DC sweep resistance measurement of CNT coating, removed from copper substrate, in different current ranges. The voltage overflow happens at a value of  $\sim 5.2 \times 10^{-3} \text{A}$  while the voltage does not exceed values more than 120mV, which is far lower than the limits of the device. Experiments 13-18 in this set show that this phenomenon is reversible and does not affect the properties of the CNT coating.

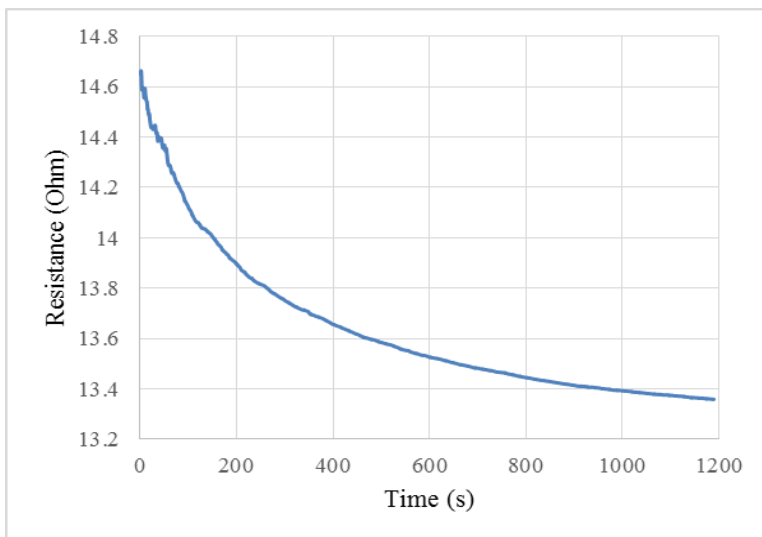


Figure 4-6: Resistance vs. time measurements for composite CNT coated Nylon wire. The initial resistance of 14.65  $\Omega$  and final resistance of 13.36  $\Omega$  after 20 minutes. Method of measurement is 4 probe.



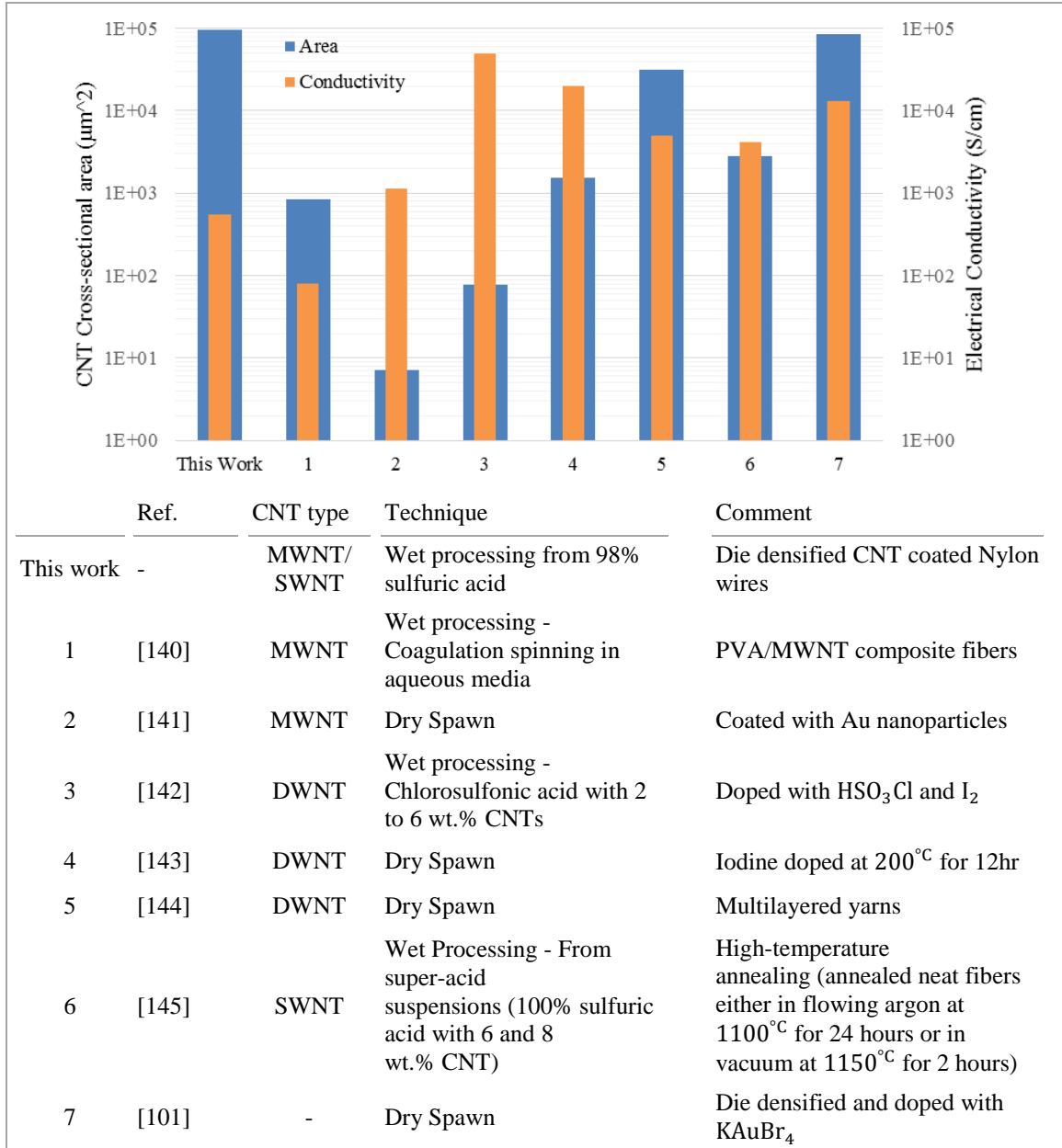


Figure 4-7: Electrical conductivity vs. CNT fiber area results from our studies and comparison with a selection of best results published for CNT fibers and wires. The data shown in this chart is for CNT coating cross-section only.

## CHAPTER 5 : STRUCTURAL CHARACTERIZATION OF CNT WIRES

Structure of the different CNT wires was investigated using light microscopy, scanning electron microscopy (SEM), and Raman spectroscopy. SEM was used to visually probe the alignment of the vertically aligned carbon nanotubes used for preparing the solutions, and for side and cross-sectional imaging of the wire specimens. Micro Raman spectroscopy was used to investigate the quality of the raw carbon nanotubes as well as CNT coatings. Polarized Raman was used to determining the level of alignment of the CNTs along the wires.

### 5.1. Microscopy

Cross-sectional microscopy specimens were prepared to measure the substrate diameter, coating thickness, and probe the CNT microstructure. Portions of each wire were cut and placed vertically into a polystyrene mold, which was then filled with the Aeropoxy PR2032/PH3670. Samples were degassed under the vacuum and cured overnight at room temperature and post-cured at 80 °C for two hours. The samples were subsequently subjected to a grinding and polishing, following standard metallography procedures. Abrasive papers with 240, 400, 600 and 1000 grit size were used for grinding followed by polishing with 6 and 1 $\mu$ m diamond paste. Samples were observed under a light microscope and gold coated for scanning electron microscopy (SEM). An FEI Quanta 3D FEG SEM was used for imaging. Low magnification images were used to confirm substrate and coating diameters, and high magnification images were used to characterize alignment, porosity, and structure of the CNT coating.

## 5.2. Scanning Electron Microscopy

### *SEM of MWCNTs*

SEM results from the vertically aligned CNTs grown with our chemical vapor deposition apparatus show that the forests reach  $800\mu\text{m}$  –  $1\text{mm}$  in height for the duration of the growth. The diameter of these CNTs were  $13\text{-}30\text{nm}$  and they exhibited waviness. Figure 5-1 show these CNT structures at various resolutions. It's noteworthy that their waviness worsens toward the tip of the forest and roots adjacent to the substrate. The vertically aligned carbon nanotube forests from GeneralNano possess a similar structure as the ones that were grown in-house, although, they look more entangled.

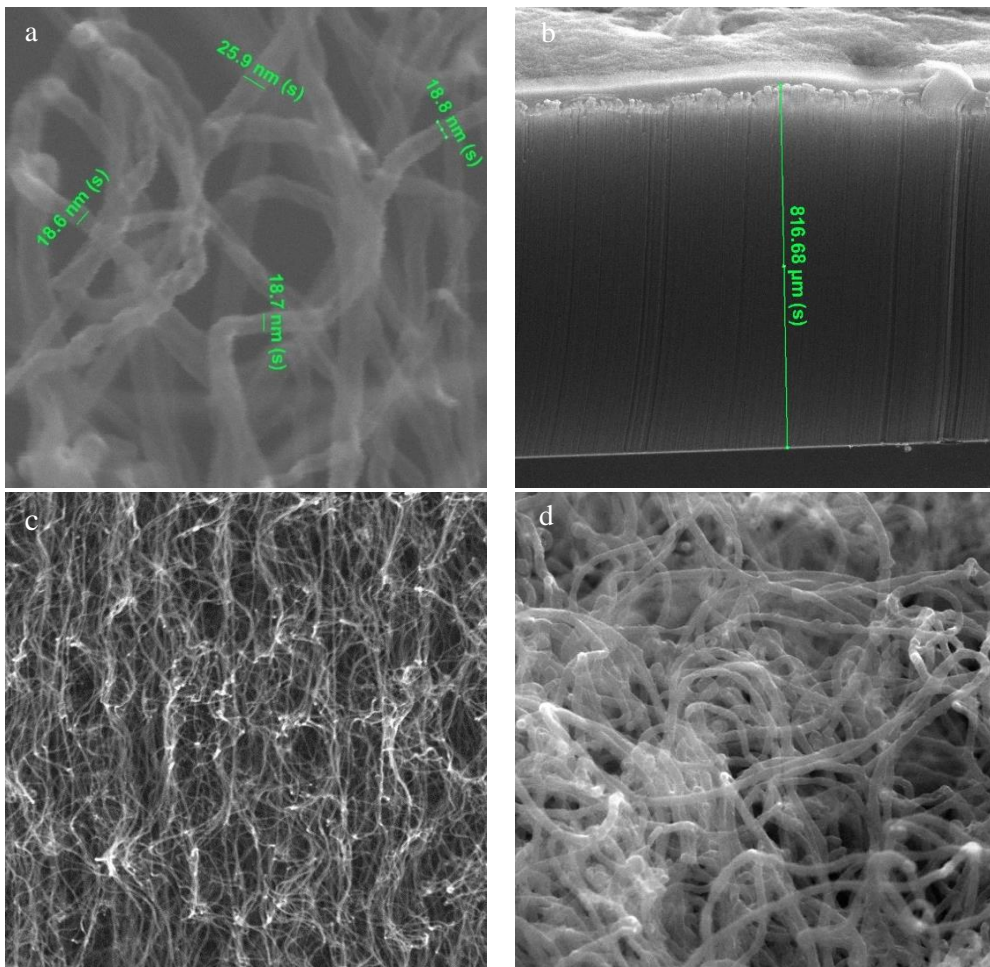


Figure 5-1: Scanning Electron Microscopy of pristine MWCNTs at a) 500K $\times$  magnification. b)  $\sim$ 200 $\times$  magnification. c) 20K $\times$  magnification. From the side view of the forest and d) 50K $\times$  magnification from top of the batch.

*SEM of CNT coated copper wires*

Cross-sectional samples were gold coated prior to SEM imaging. The gold coating layer is in the order of nanometers. SEM results from the sides of the prepared CNT coatings on copper wires show a relatively good alignment (Figure 5-2-d). Figure 5-2 shows a comparison between the as-synthesized CNT forests and the bundles formed in the solution and deposited on a copper substrate. The uniformity of the coating is in good agreement with our laser micrometry measurements.

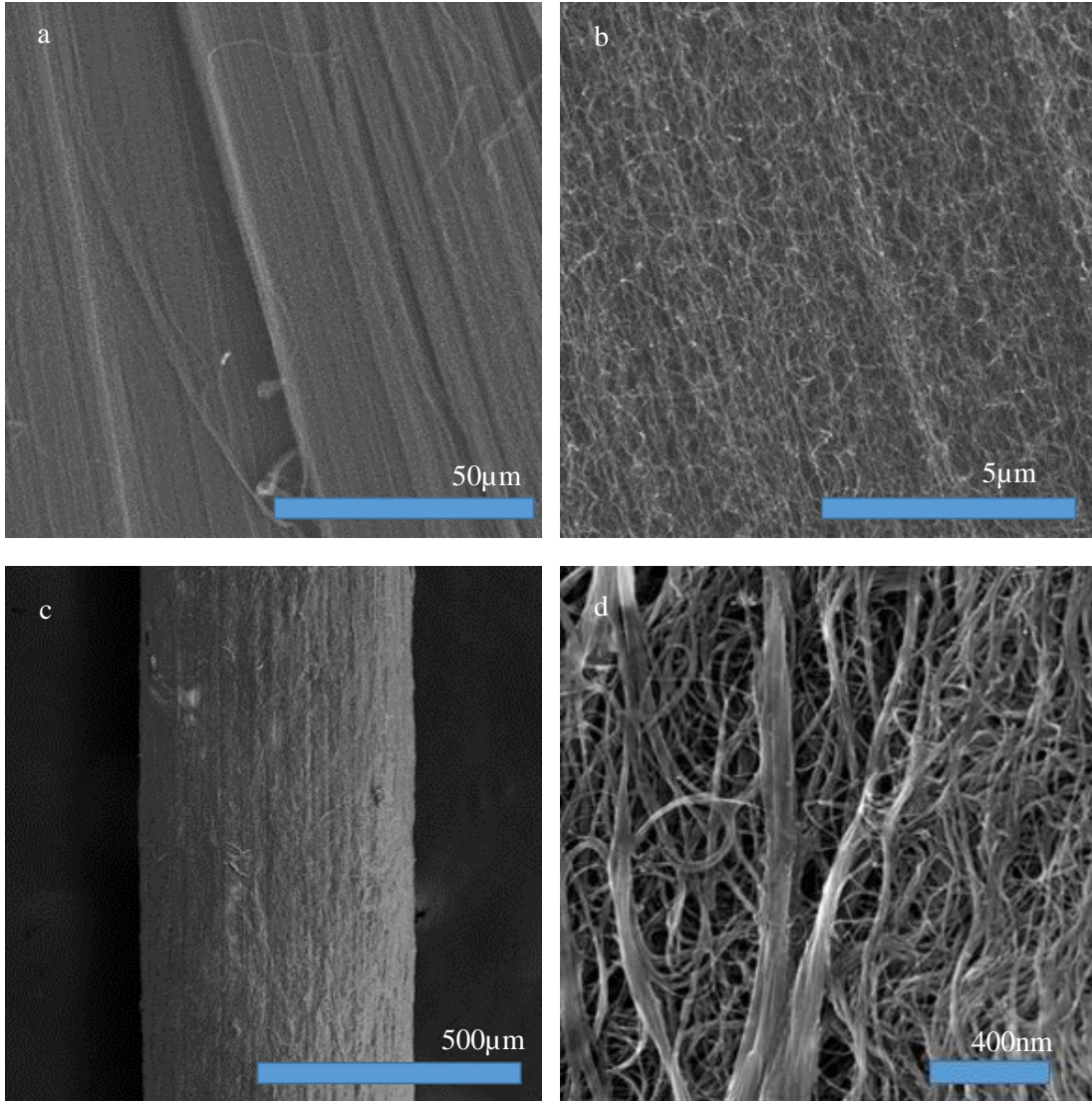


Figure 5-2: a and b) SEM images of General Nano MWCNT forests in different magnifications where entanglement is observable between nanotubes. c) a CNT coated copper wire after several wire drawing steps. d) the MWCNT bundles formed on the copper substrate and aligned in the direction of the long axis of the wire in c.

Cross-sectional SEM images of the coated copper wires are shown in

Figure 5-3. Misalignment of the center of the coating and copper substrate was observed for some of the samples, specifically with thicker coatings. This may be due to different

sources such as the slight angle of extrusion of wire from the solution or misalignment of the wire in the die drawing process. As shown in Figure 5-3, the coating is not connected to the core in some regions. CNT coated nylon wires showed a composite layer of nylon with CNTs embedded (Figure 3-9). The porous structure formed on the outer surface of nylon seems to adhere well to the coating. This layer is the reason for better attachment of CNTs to the nylon wires during solution coating. However, the infusion of polymer in CNTs decreased the coating electrical conductivity.

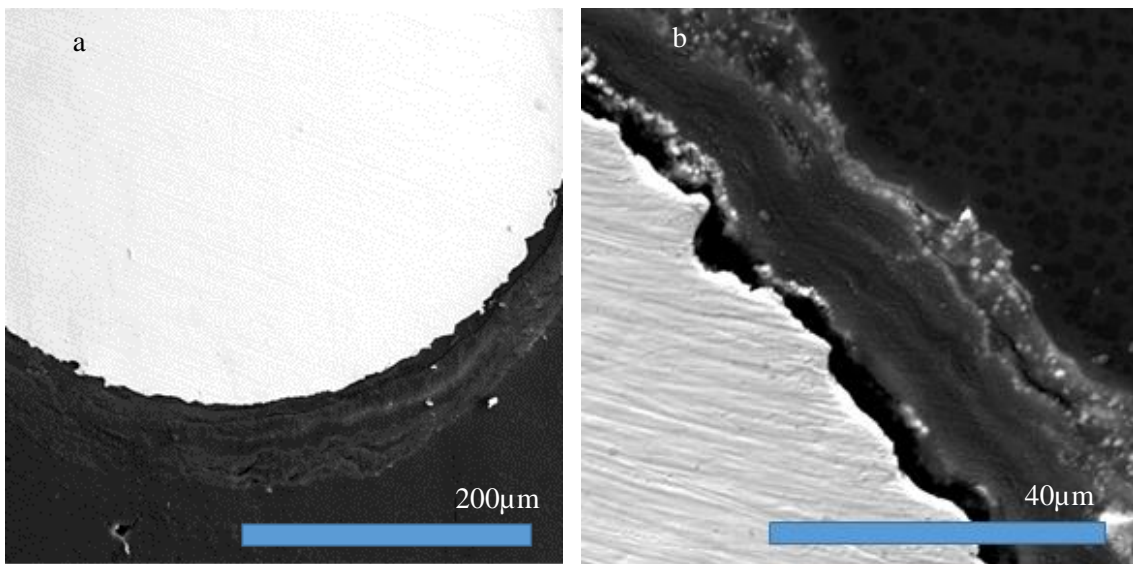


Figure 5-3: a) Cross-section of CNT coated copper composite wire prepared with MWNT solution. b) A gap between CNT coating and copper substrate is visible in some areas of cross-sections.

*SEM of CNT coated Nylon wires*

Cross-sectional images of the CNT coatings on nylon wires (Figure 5-4) are less eccentric than their copper counterparts. Similar CNT alignment for coatings on both nylon and copper were observed.

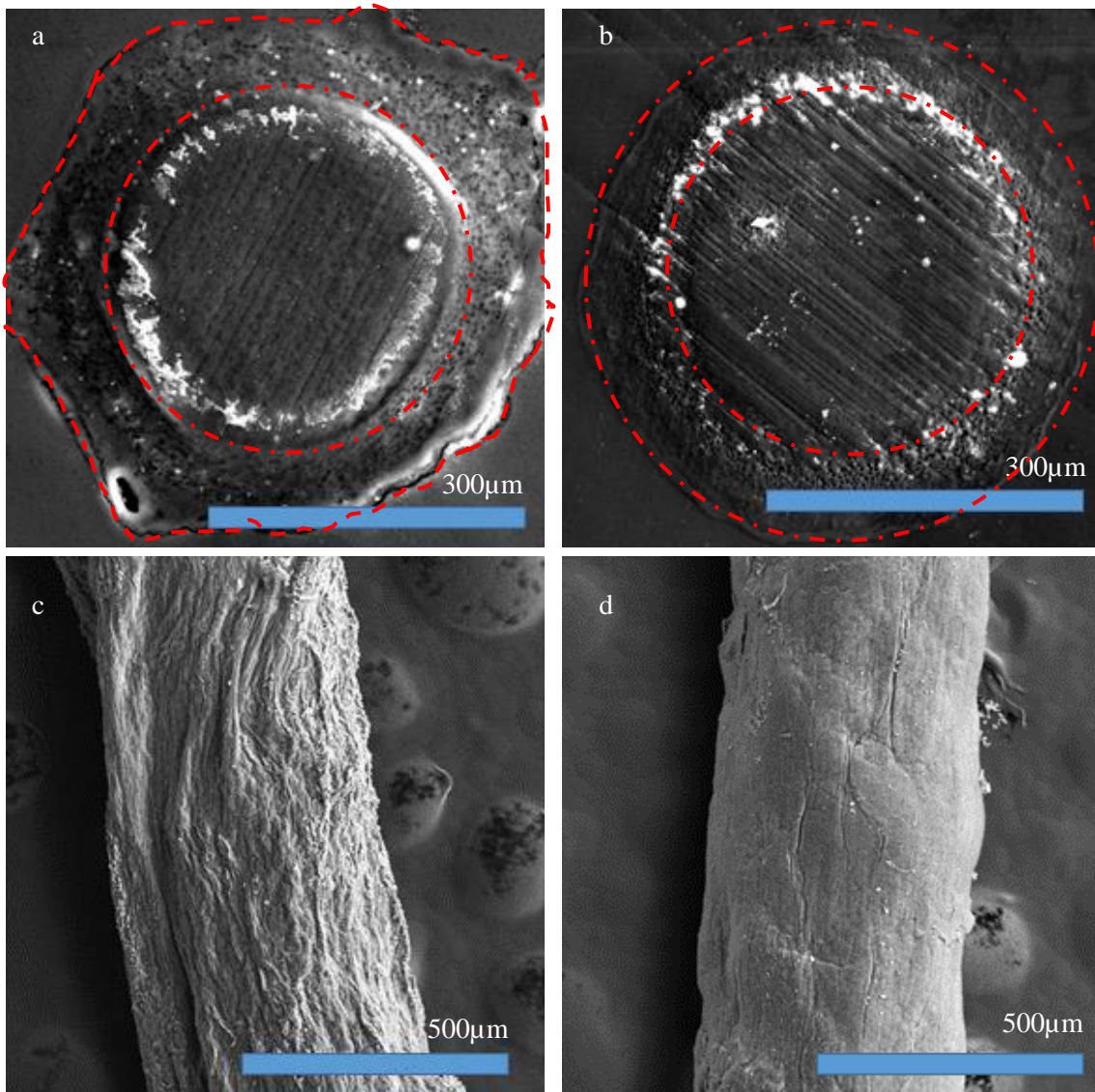


Figure 5-4: Cross-sectional SEM images of CNT coated nylon wires without die drawing (a) and with die drawing (b). SEM of the surface of CNT coated nylon wires with no die drawing (c) and with die drawing (d).

### 5.3. Raman spectroscopy

In Raman spectroscopy, absorbing a photon causes electron excitation from the valence band to the conduction energy band, and subsequently, the electron emits or absorbs a phonon and finally returns to the valence energy band by emitting a photon.[146] Plotting the intensity of this scattered light versus its energy loss results in the Raman spectrum. The energy loss in the plot is called the frequency downshift, and the peaks of the spectra can provide information about the bonds and chirality of carbon nanotubes.[147] In an SWCNT Raman spectrum, the radial breathing mode (RBM) contains information about the diameter of the CNTs and therefore is an evidence of the existence of SWCNTs in the sample. RBM and G band are considered first order Raman modes for CNTs. Also, the ratio of the semiconducting and metallic SWCNTs in a sample can be estimated using multiple laser energies. The G band in an SWCNT Raman spectrum includes several peaks since the two carbon atoms in a unit cell of SWCNT are positioned in a cylindrical manner. The two significant peaks in G band are  $G^+$  and  $G^-$ . The  $G^+$  corresponds to the atomic vibrations along the axis and is positioned around  $1590\text{cm}^{-1}$ . The  $G^-$  peak on the other hand, shows the circumferential vibrations of atoms and its frequency is around  $1570\text{cm}^{-1}$ . The double-resonance Raman features of CNTs corresponds to the D and  $G'$  bands with frequencies around  $1350\text{cm}^{-1}$  and  $2700\text{cm}^{-1}$ , respectively. D-band peak corresponds to disorder in CNTs.[147]

#### *Raman spectroscopy of MWCNTs*

In the Raman spectra of multi-walled carbon nanotubes, the RBM mode is usually broadened over a range of frequencies and usually exhibits a low intensity. Also, the



diameter distribution of the CNTs in MWCNTs results in a narrower splitting of the  $G^+$  and  $G^-$  bands, and as a result, the G band shows an asymmetric peak around  $1582\text{cm}^{-1}$ . The excitation wavelength of Raman spectroscopy has a minor influence over the frequency downshift and peak location in the Raman spectra.[148] Our Raman experiments were carried out using a  $532\text{nm}$  laser. More information regarding the location of bands with these two wavelengths can be found in the studies of Asthana et al.[148] The existence of defects on nanotubes sidewalls results in changes in the D-band. The addition of other chemical species to the sidewalls may result in charge transfer to the nanotube, exhibiting a downshift or upshift in various Raman modes.

Figure 5-5 and Figure 5-6 show Raman spectra of MWCNTs used in this study in their pristine form and after dispersion in sulfuric acid and deposition on wires. There is almost no change in the G/D peak ratios, which indicates the processing had no effect on nanotubes.

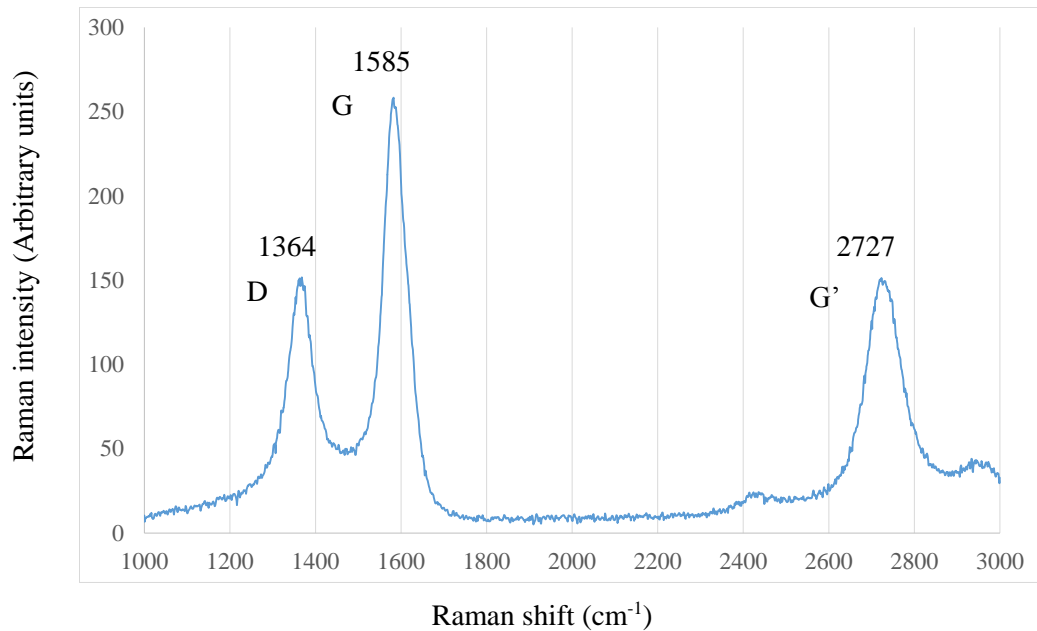


Figure 5-5: Raman spectroscopy of the pristine MWCNT forests

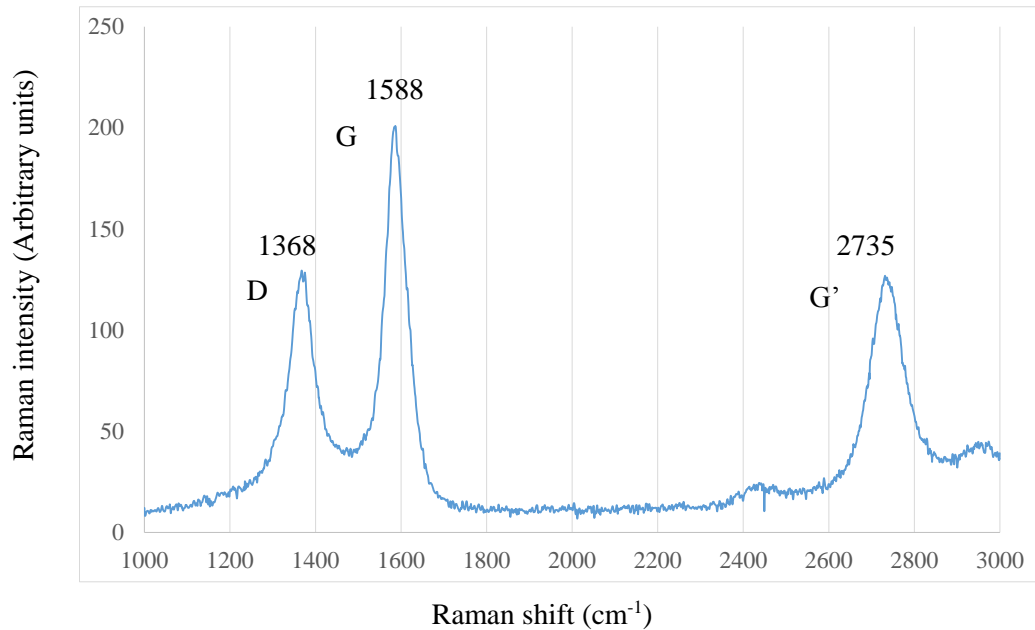


Figure 5-6: Raman spectroscopy of MWCNT coating on nylon wire prepared from CNT/sulfuric acid solution dip-coating process.

#### *Polarized Raman spectroscopy*

CNT alignment can be determined via polarized Raman spectroscopy. This measurement can qualitatively probe alignment in CNT wires. Studies show that at the angle of 55 degrees between the polarization direction and nanotubes axis, the G' band intensity shows its minimum value and the maximum value is achieved at the 0 degrees.

Figure 5-7 shows polarized Raman spectroscopy of CNT coated nylon wires.

For this study, a sample of aligned CNT sheet was used to verify the measurement. The long axis of the wire is parallel to the zero degrees polarization direction. The z-axis was used to focus the laser to acquire the highest intensity per second. The exposure time is determined from the intensity. At each location, multiple measurements were taken at different angles (0, 20, 40, 50, 60, 90, 180) (Figure 5-7). At least five measurements were taken on each sample from five locations.

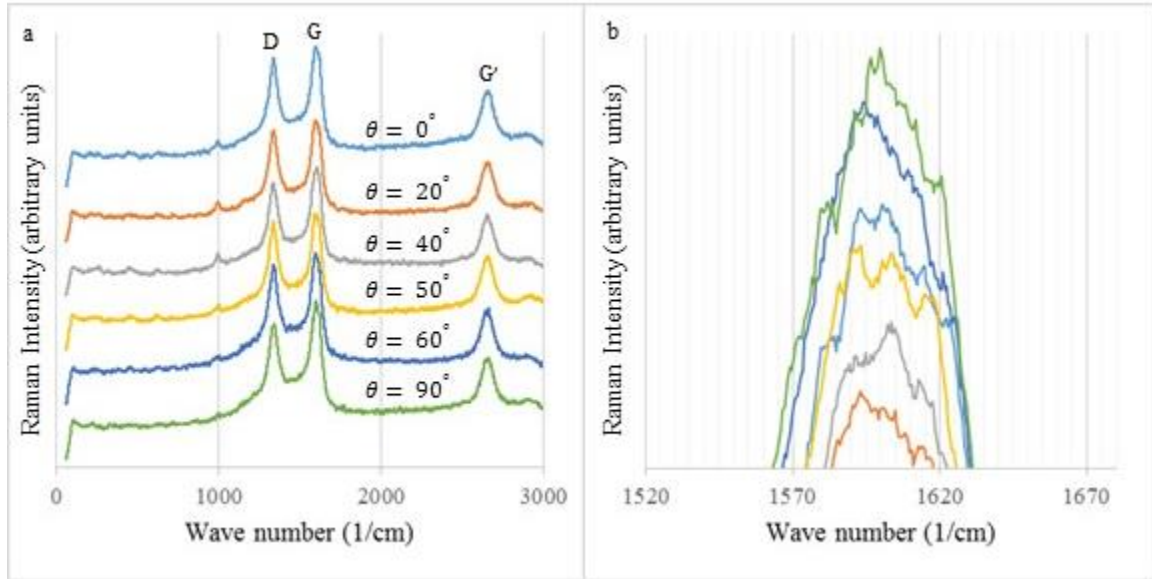


Figure 5-7 - Polarized Raman spectroscopy of CNT coated Nylon sample from MWCNT solution as a function of measured angles 0, 20, 40, 50, 60, 90 degrees of polarization direction.

Studies show that the intensity of G band in aligned MWCNT fibers show a decrease over 0-55 degree in polarization angle (The G-band disappears at 55 degrees) and then increase in 55-90 degree to about 0.6 times the initial intensity at zero degrees.[149] In case of SWCNT fibers, the G-band intensity has a decrease over the range of 0-90 degrees polarization angle.[150, 151] In the case of our reference sample, which was a sheet of highly aligned MWCNTs, Raman intensities at 0 and 90 degrees have the highest values, and at 55 degrees, a slight decrease in the G-band intensity was observed (Figure 5-8). Polarized Raman spectroscopy of our wire samples (from nylon substrate, copper substrate, MWCNT solution, or MWCNT/SWCNT solution) show almost the same pattern in their G-band intensities (Figure 5-8). In the case of less aligned coatings, a slight decrease in G-band intensity of Raman spectra from 55 degrees is observed (Figure 5-9). The band intensities in MWCNT/SWCNT samples are overruled by SWNTs in the spectra. Although, only a slight change in the order of

intensity peaks from different polarization directions into the correct order of alignment is observed (Figure 5-10). This misalignment may be due to the fact that the dip-coating process is not yet optimized to form highly aligned thick coatings and the die drawing process also mostly affects the outer surface of the coatings.

Pre-processed SWCNTs used in this study possess a  $I_G/I_D$  ratio of 50. Variations in the amount of MWCNTs and SWCNTs under the area of Raman spectroscopy contributes to the differences in the values of  $I_G/I_D$  ratio in samples from MWCNT/SWCNT solution. But the  $I_G/I_D$  ratio is consistently 1.12 with the samples from MWCNT solution.

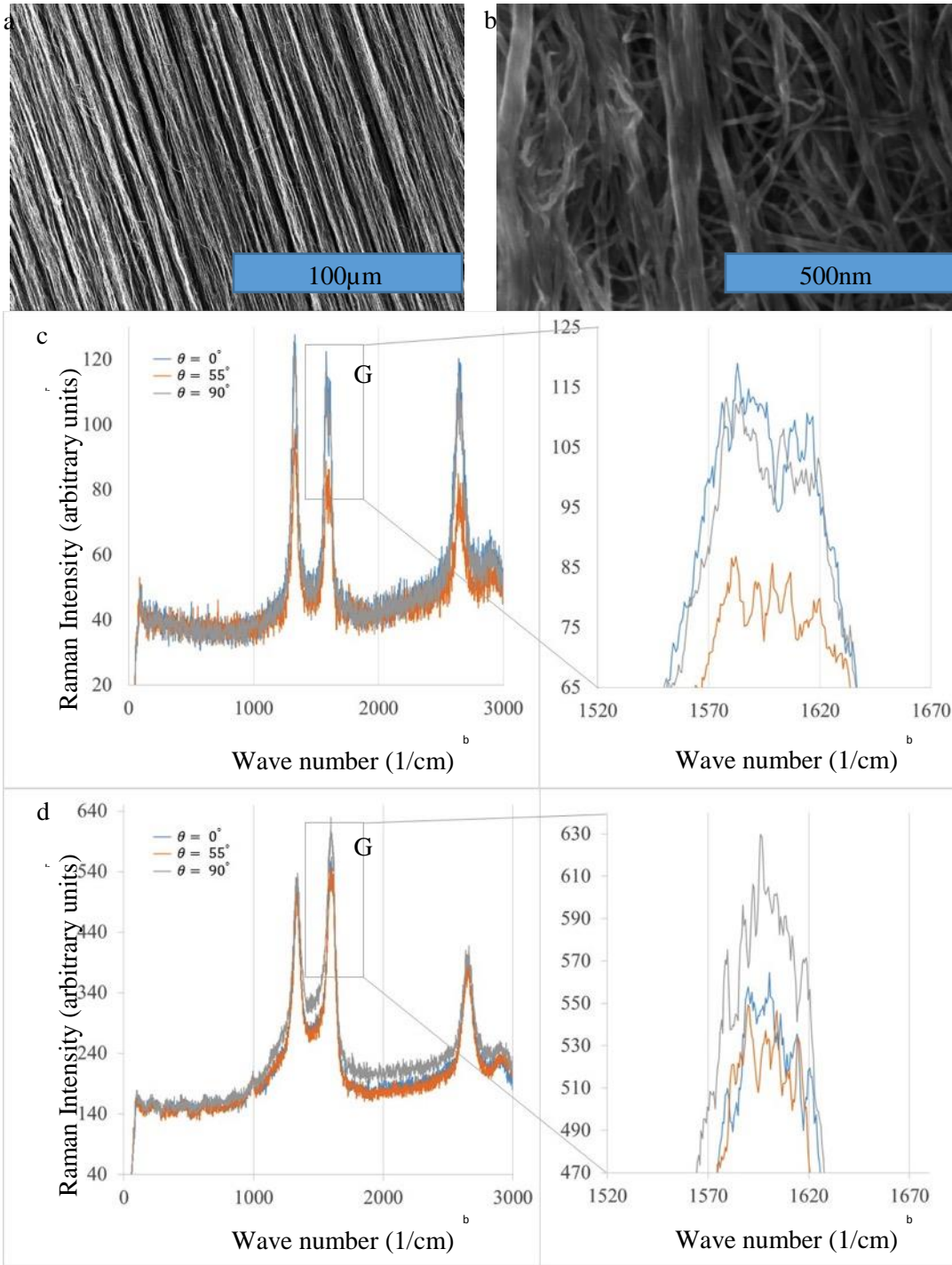


Figure 5-8: SEM (a) and polarized Raman spectroscopy(c) of aligned MWCNT sheet with zoomed in G-band intensities at 0,55, and 90 degree polarization direction compared to SEM (b) and polarized Raman spectroscopy (d) of an MWCNT coated nylon wire prepared by the method described in this work.

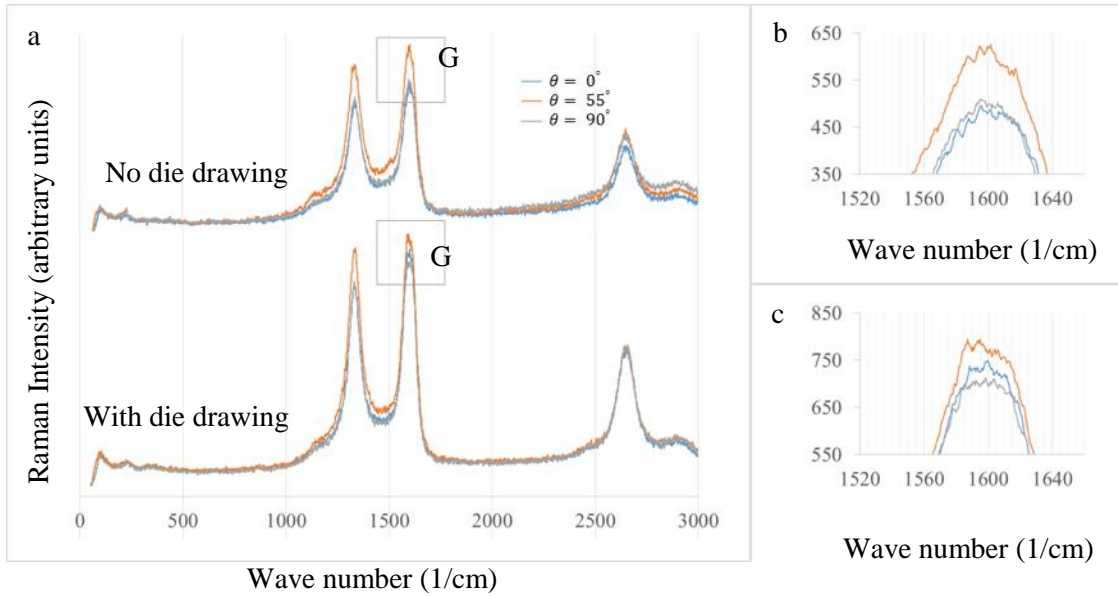


Figure 5-9: Polarized Raman spectroscopy of CNT coated Copper sample from MWCNT solution, with and without die drawing process

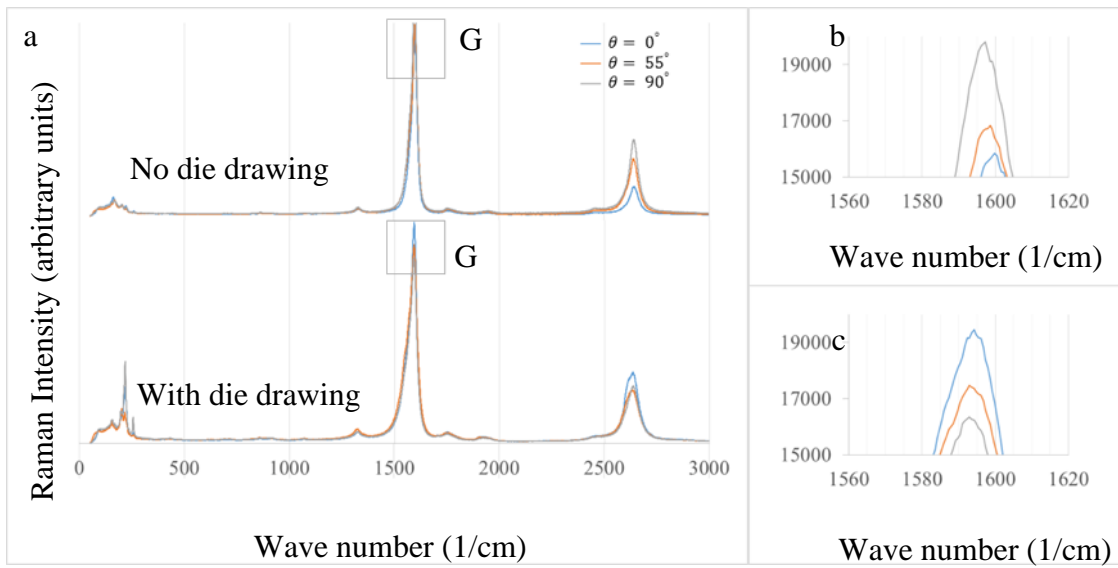


Figure 5-10: Polarized Raman spectroscopy of CNT coated nylon sample from MWCNT/SWCNT solution, with and without die drawing process

## CHAPTER 6 : CONCLUSIONS AND FUTURE WORK

### 6.1. Conclusions

The scalable solution coating and wire drawing method introduced in this study proved to be an effective approach for coating various wire substrates with ultra-long CNTs. The challenge remains to achieve better alignment and packing and enhance CNT-substrate wire interface adhesion, thus electrical properties comparable to copper and aluminum. Sulfuric acid showed to be an effective dispersant for long multi-wall carbon nanotubes where it facilitated CNT fiber formation and didn't affect the CNT structure. Based on the measured electrical conductivities, quality of the precursor CNTs is the dominant parameter for the performance of a macro-scale conductor; the 46.8% increase in conductivity of the samples from SWCNT/MWCNT solution over samples from MWCNT solution as well as other studies[100] show that by using precursor CNTs with better characteristics such as higher lengths (higher dimensional aspect ratio), and purity (Higher  $I_G/I_D$  ratio in Raman), much enhanced CNT conductors can be fabricated by this method. Scanning electron microscopy of the coatings showed good levels of CNT alignment and packing. Light microscopy of the cross-sections of the coatings as well as their side view showed improvement of diameter uniformity of the coatings after die drawing. Raman spectroscopy confirmed that the method almost did not cause any damage to the CNTs and based on the polarized Raman spectroscopy results, there is still room for improvement of alignment of the CNT structures, especially for thicker coatings. Figure 6-1 is a representative of the manufacturing process from the nano-scale nanotubes to the macro-scale wires.

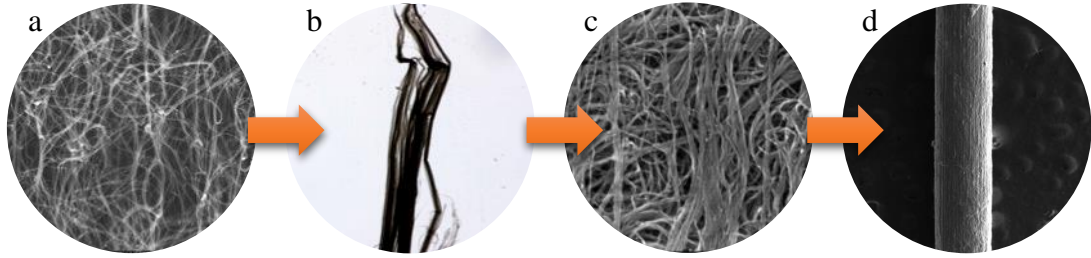


Figure 6-1: From individual MWCNTs to coatings of tens of microns in thickness. a) MWCNT forest at 300K $\times$  magnification. b) MWCNT fiber in sulfuric acid solution. c) Formation of MWCNT bundles on the surface of the coating. d) 69 $\mu$ m thick MWCNT coating on a 24AWG copper wire at 100 $\times$  magnification.

## 6.2. Future Work

Some questions remained unanswered in this research, such as the behavior seen in electrical resistance measurement of the coatings, CNT-copper interface nature, and interactions between the CNT bundles in solution and during wire drawing. Cross-sectional images of CNT coated nylon wires showed that there is an interface layer formed where nanotubes and nylon are mixed. Also, the removed CNT layers from copper wires show a trace of redness on their inner surface that can be attributed to partial dissolution of copper in sulfuric acid. Although, both cases resulted in similar conductivities of CNT coatings. But it's important to better understand the effects of different substrates on the structure and properties of the CNT coatings.

It is crucial to optimize many aspects of the process to achieve higher conductivity coatings. It would also be interesting to investigate other applications of the CNT coated wires such as electromagnetic shielding, thin film antennas, and composite electrodes. First of all, a better understanding of the CNT synthesis would help optimize the process. For example, controlling the chirality and selective growth of ultralong



SWCNTs and DWCNTs with higher qualities and less waviness is only possible through this. Also, our understanding of the interactions between ultralong CNTs with different acids is limited. Adhesion mechanism of CNTs on different materials seems to be another area of importance. Exclusive to this process, understanding the rheology of CNT dispersions and their dip-coating process would lead to the production of more aligned coatings and scaling up of the process. It would be of utmost importance to understand the alignment mechanism, in particular, whether alignment is due to shear forces from surface tension upon extraction from solution or because of the vortex alignment in the solution. Not to mention, the mechanisms behind the capillary assembly of CNTs are also missing. Studies can be further carried out to better characterize the electrical properties of the coatings at different temperatures as well as thermal and mechanical properties of the coatings.

## BIBLIOGRAPHY

1. Matula, R.A., *Electrical-Resistivity of Copper, Gold, Palladium, and Silver*. Journal of Physical and Chemical Reference Data, 1979. **8**(4): p. 1147-1298.
2. Peters, D.T. and K.J.A. Kundig, *Selecting Coppers and Copper-Alloys*. Advanced Materials & Processes, 1994. **145**(6): p. 20-26.
3. Farag, M.M., *Quantitative Methods of Materials Selection*. 2006: p. 466-488.
4. Ashby, M.F. and D. Cebon, *Materials Selection in Mechanical Design*. Journal De Physique Iv, 1993. **3**(C7): p. 1-9.
5. *EERE: Funding Opportunity Announcement (FOA) Number: DE-FOA-0001467*, U.D.o. Energy, Editor. 2016.
6. III, W.B., *Aircraft Wire and Cable: Doing More With Less*, in *Avionics Today*. 2014.
7. Holesinger, T.G., DePaula, R., Rowley, J., Sperling, K., & Pappas, J. M. *Carbon Nanotube Composite Cables for Ultra-Deepwater Oil and Gas Fields*. in *Offshore Technology Conference*. 2014.
8. Janas, D., A.C. Vilatela, and K.K.K. Koziol, *Performance of carbon nanotube wires in extreme conditions*. Carbon, 2013. **62**: p. 438-446.
9. Neher, J.H., and M. H. McGrath, *The calculation or the temperature rise and load capability of cable systems*. RATIO, 1994. **50.2**.
10. Iijima, S., *Helical microtubules of graphitic carbon*. Nature, 1991. **354**: p. 56-58.
11. Suzuura, H. and T. Ando, *Phonons and electron-phonon scattering in carbon nanotubes*. Physical Review B, 2002. **65**(23).
12. Park, J.Y., et al., *Electron-phonon scattering in metallic single-walled carbon nanotubes*. Nano Letters, 2004. **4**(3): p. 517-520.
13. Hu, L.B., D.S. Hecht, and G. Gruner, *Carbon Nanotube Thin Films: Fabrication, Properties, and Applications*. Chemical Reviews, 2010. **110**(10): p. 5790-5844.
14. De Volder, M.F.L., et al., *Carbon Nanotubes: Present and Future Commercial Applications*. Science, 2013. **339**(6119): p. 535-539.
15. White, C.T. and T.N. Todorov, *Carbon nanotubes as long ballistic conductors*. Nature, 1998. **393**(6682): p. 240-242.
16. Dekker, C., *Carbon nanotubes as molecular quantum wires*. Physics Today, 1999. **52**(5): p. 22-28.
17. Shokrieh, M.M. and R. Rafiee, *A review of the mechanical properties of isolated carbon nanotubes and carbon nanotube composites*. Mechanics of Composite Materials, 2010. **46**(2): p. 155-172.
18. Zhong, G., Iwasaki, T., Robertson, J., & Kawarada, H., *Growth kinetics of 0.5 cm vertically aligned single-walled carbon nanotubes*. The Journal of Physical Chemistry B, 111(8), 2007: p. 1907-1910.
19. Xiang, R., Luo, G., Yang, Z., Zhang, Q., Qian, W., & Wei, F., *Temperature effect on the substrate selectivity of carbon nanotube growth in floating chemical vapor deposition*. Nanotechnology, 18(41), 415703, 2007.
20. Li, Y., Xu, G., Zhang, H., Li, T., Yao, Y., Li, Q., & Dai, Z., *Alcohol-assisted rapid growth of vertically aligned carbon nanotube arrays*. Carbon, 91, 45-55., 2015.

21. Eres, G., Kinkhabwala, A. A., Cui, H., Geohegan, D. B., Poretzky, A. A., & Lowndes, D. H., *Molecular beam-controlled nucleation and growth of vertically aligned single-wall carbon nanotube arrays*. The Journal of Physical Chemistry B, 109(35), 16684, 2005.
22. Xu, Y.Q., Flor, E., Kim, M. J., Hamadani, B., Schmidt, H., Smalley, R. E., & Hauge, R. H., *Vertical array growth of small diameter single-walled carbon nanotubes*. Journal of the American Chemical Society, 128(20), 6560-6561, 2006.
23. Zhang, G., Mann, D., Zhang, L., Javey, A., Li, Y., Yenilmez, E., ... & Dai, H. . *Ultra-high-yield growth of vertical single-walled carbon nanotubes: Hidden roles of hydrogen and oxygen*. Proceedings of the National Academy of Sciences of the United S, Zhang, G., Mann, D., Zhang, L., Javey, A., Li, Y., Yenilmez, E., ... & Dai, H. (2005). *Ultra-high-yield growth of vertical single-walled carbon nanotubes: Hidden roles of hydrogen and oxygen*. Proceedings of the National Academy of Sciences of the United S. Proceedings of the National Academy of Sciences of the United States of America, 102(45), 16141-16145, 2005.
24. Hata, K., Futaba, D. N., Mizuno, K., Namai, T., Yumura, M., & Iijima, S., *Water-assisted highly efficient synthesis of impurity-free single-walled carbon nanotubes*. Science, 306(5700), 1362-1364, 2004.
25. Noda, S., Hasegawa, K., Sugime, H., Kakehi, K., Zhang, Z., Maruyama, S., & Yamaguchi, Y., *Millimeter-thick single-walled carbon nanotube forests: Hidden role of catalyst support*. Japanese journal of applied physics, 46(5L), L399, 2007.
26. Yasuda, S., Futaba, D. N., Yamada, T., Satou, J., Shibuya, A., Takai, H., ... & Hata, K., *Improved and large area single-walled carbon nanotube forest growth by controlling the gas flow direction*. ACS Nano, 3(12), 4164-4170, 2009.
27. Wang, X., Li, Q., Xie, J., Jin, Z., Wang, J., Li, Y., ... & Fan, S., *Fabrication of ultralong and electrically uniform single-walled carbon nanotubes on clean substrates*. nano letters, 9(9), 3137-3141, 2009.
28. Huang, S., Woodson, M., Smalley, R., & Liu, J., *Growth mechanism of oriented long single walled carbon nanotubes using "fast-heating" chemical vapor deposition process*. Nano Letters, 4(6), 1025-1028, 2004.
29. Zheng, L.X., O'connell, M. J., Doorn, S. K., Liao, X. Z., Zhao, Y. H., Akhadov, E. A., ... & Zhu, Y. T., *Ultralong single-wall carbon nanotubes*. Nature materials, 3(10), 673-676, 2004.
30. Parker, D.H., et al., *High-Yield Synthesis, Separation, and Mass-Spectrometric Characterization of Fullerenes C60 to C266*. Journal of the American Chemical Society, 1991. **113**(20): p. 7499-7503.
31. Baddour, C. and C. Briens, *Carbon nanotube synthesis: A review*. International Journal of Chemical Reactor Engineering, 2005. **3**.
32. Scott, C.D., et al., *Growth mechanisms for single-wall carbon nanotubes in a laser-ablation process*. Applied Physics a-Materials Science & Processing, 2001. **72**(5): p. 573-580.
33. Unrau, C.J., V.R. Katta, and R.L. Axelbaum, *Characterization of diffusion flames for synthesis of single-walled carbon nanotubes*. Combustion and Flame, 2010. **157**(9): p. 1643-1648.

34. Diener, M.D., N. Nicholson, and J.M. Alford, *Synthesis of single-walled carbon nanotubes in flames*. Journal of Physical Chemistry B, 2000. **104**(41): p. 9615-9620.
35. Hu, W.C., S.S. Hou, and T.H. Lin, *Analysis on Controlling Factors for the Synthesis of Carbon Nanotubes and Nano-Onions in Counterflow Diffusion Flames*. Journal of Nanoscience and Nanotechnology, 2014. **14**(7): p. 5363-5369.
36. Liu, Y.C., B.M. Sun, and Z.Y. Ding, *Effect of hydrogen on V-type pyrolysis flame synthesis of carbon nanotubes*. Advanced Polymer Science and Engineering, 2011. **221**: p. 545-549.
37. Cassell, A.M., et al., *Large scale CVD synthesis of single-walled carbon nanotubes*. Journal of Physical Chemistry B, 1999. **103**(31): p. 6484-6492.
38. Kumar, M. and Y. Ando, *Chemical Vapor Deposition of Carbon Nanotubes: A Review on Growth Mechanism and Mass Production*. Journal of Nanoscience and Nanotechnology, 2010. **10**(6): p. 3739-3758.
39. Yamamoto, S., et al., *Synthesis of single walled carbon nanotubes by laser vaporized Catalytic Chemical Vapor Deposition technique*. Proceedings of the Asme/Jsme Thermal Engineering Summer Heat Transfer Conference 2007, Vol 2, 2007: p. 387-393.
40. Xue, R.L., et al., *Large-scale Synthesis of Nitrogen-doped Carbon Nanotubes by Chemical Vapor Deposition Using a Co-based Catalyst from Layered Double Hydroxides*. Catalysis Letters, 2010. **135**(3-4): p. 312-320.
41. Campos-Delgado, J., et al., *Chemical Vapor Deposition Synthesis of N-, P-, and Si-Doped Single-Walled Carbon Nanotubes*. ACS Nano, 2010. **4**(3): p. 1696-1702.
42. Watanabe, T., et al., *Microwave plasma chemical vapor deposition synthesis of boron-doped carbon nanotube*. Physica C-Superconductivity and Its Applications, 2010. **470**: p. S608-S609.
43. Unalan, H.E. and M. Chhowalla, *Investigation of single-walled carbon nanotube growth parameters using alcohol catalytic chemical vapour deposition*. Nanotechnology, 2005. **16**(10): p. 2153-2163.
44. Hata, K., et al., *Water-Assisted Highly Efficient Synthesis of Impurity-Free Single-Walled Carbon Nanotubes*. Science, 2004. **306**(5700): p. 1362-1364.
45. Song, L., et al., *Large-scale synthesis of rings of bundled single-walled carbon nanotubes by floating chemical vapor deposition*. Advanced Materials, 2006. **18**(14): p. 1817-+.
46. Peng, B.H., et al., *Enrichment of metallic carbon nanotubes by electric field-assisted chemical vapor deposition*. Carbon, 2011. **49**(7): p. 2555-2560.
47. Ikuno, T., et al., *Selective growth of straight carbon nanotubes by low-pressure thermal chemical vapor deposition*. Japanese Journal of Applied Physics Part 1- Regular Papers Brief Communications & Review Papers, 2004. **43**(2): p. 860-863.
48. Venegoni, D., et al., *Parametric study for the growth of carbon nanotubes by catalytic chemical vapor deposition in a fluidized bed reactor*. Carbon, 2002. **40**(10): p. 1799-1807.
49. Qin, L.C., et al., *Growing carbon nanotubes by microwave plasma-enhanced chemical vapor deposition*. Applied Physics Letters, 1998. **72**(26): p. 3437-3439.

50. Okazaki, T. and H. Shinohara, *Synthesis and characterization of single-wall carbon nanotubes by hot-filament assisted chemical vapor deposition*. Chemical Physics Letters, 2003. **376**(5-6): p. 606-611.
51. Pirard, S.L., J.P. Pirard, and C. Bossuot, *Modeling of a Continuous Rotary Reactor for Carbon Nanotube Synthesis by Catalytic Chemical Vapor Deposition*. Aiche Journal, 2009. **55**(3): p. 675-686.
52. Dupuis, A., *The catalyst in the CCVD of carbon nanotubes—a review*. Progress in Materials Science, 2005. **50**(8): p. 929-961.
53. Barzegar, H.R., et al., *Simple Dip-Coating Process for the Synthesis of Small Diameter Single-Walled Carbon Nanotubes—Effect of Catalyst Composition and Catalyst Particle Size on Chirality and Diameter*. Journal of Physical Chemistry C, 2012. **116**(22): p. 12232-12239.
54. Zhou, K., et al., *Multi-Directional Growth of Aligned Carbon Nanotubes Over Catalyst Film Prepared by Atomic Layer Deposition*. Nanoscale Research Letters, 2010. **5**(10): p. 1555-1560.
55. Wei, Y.Y., et al., *Effect of catalyst film thickness on carbon nanotube growth by selective area chemical vapor deposition*. Applied Physics Letters, 2001. **78**(10): p. 1394-1396.
56. Gan, B., et al., *Y-junction carbon nanotubes grown by in situ evaporated copper catalyst*. Chemical Physics Letters, 2001. **333**(1-2): p. 23-28.
57. Lee, S.Y., M. Yamada, and M. Miyake, *Synthesis of carbon nanotubes over gold nanoparticle supported catalysts*. Carbon, 2005. **43**(13): p. 2654-2663.
58. Wong, Y.M., et al., *Carbon nanotubes field emission devices grown by thermal CVD with palladium as catalysts*. Diamond and Related Materials, 2004. **13**(11-12): p. 2105-2112.
59. Han, J.H., et al., *Growth characteristics of carbon nanotubes using platinum catalyst by plasma enhanced chemical vapor deposition*. Diamond and Related Materials, 2003. **12**(3-7): p. 878-883.
60. Blanco, M., et al., *Enhancing the hydrogen transfer catalytic activity of hybrid carbon nanotube-based NHC-iridium catalysts by increasing the oxidation degree of the nanosupport*. Catalysis Science & Technology, 2016. **6**(14): p. 5504-5514.
61. Fazil, A. and R. Chetty, *Synthesis and Evaluation of Carbon Nanotubes Supported Silver Catalyst for Alkaline Fuel Cell*. Electroanalysis, 2014. **26**(11): p. 2380-2387.
62. Lee, C.J., et al., *Carbon nanotubes produced by tungsten-based catalyst using vapor phase deposition method*. Chemical Physics Letters, 2002. **361**(5-6): p. 469-472.
63. Zhou, D., S. Wang, and S. Seraphin, *Single-Walled Carbon Nanotubes Grown from Yttrium Carbide Particles*. Fifty-Second Annual Meeting - Microscopy Society of America/Twenty-Ninth Annual Meeting - Microbeam Analysis Society, Proceedings, 1994: p. 772-773.
64. Flahaut, E., et al., *CCVD synthesis of carbon nanotubes from (Mg,Co,Mo)O catalysts: influence of the proportions of cobalt and molybdenum*. Journal of Materials Chemistry, 2004. **14**(4): p. 646-653.

65. Botti, S., et al., *Self-assembled carbon nanotubes grown without catalyst from nanosized carbon particles adsorbed on silicon*. Applied Physics Letters, 2002. **80**(8): p. 1441-1443.
66. Chai, S.P., S.H.S. Zein, and A.R. Mohamed, *Synthesizing carbon nanotubes and carbon nanofibers over supported-nickel oxide catalysts via catalytic decomposition of methane*. Diamond and Related Materials, 2007. **16**(8): p. 1656-1664.
67. Azam, M.A., et al., *Electrically conductive aluminum oxide thin film used as cobalt catalyst-support layer in vertically aligned carbon nanotube growth*. Advances in Natural Sciences-Nanoscience and Nanotechnology, 2015. **6**(4).
68. Dillon, A.C., et al., *A simple and complete purification of single-walled carbon nanotube materials*. Advanced Materials, 1999. **11**(16): p. 1354-1358.
69. Oncel, C. and Y. Yurum, *Carbon nanotube synthesis via the catalytic CVD method: A review on the effect of reaction parameters*. Fullerenes Nanotubes and Carbon Nanostructures, 2006. **14**(1): p. 17-37.
70. Zhang, R.F., et al., *Growth of Half-Meter Long Carbon Nanotubes Based on Schulz-Flory Distribution*. Acs Nano, 2013. **7**(7): p. 6156-6161.
71. Cho, W., Schulz, M., & Shanov, V., *Growth and characterization of vertically aligned centimeter long CNT arrays*. Carbon, 72, 264-273, 2014.
72. Futaba, D.N., et al., *Kinetics of water-assisted single-walled carbon nanotube synthesis revealed by a time-evolution analysis*. Physical Review Letters, 2005. **95**(5).
73. Amama, P.B., et al., *Role of Water in Super Growth of Single-Walled Carbon Nanotube Carpets*. Nano Letters, 2009. **9**(1): p. 44-49.
74. Tessonier, J.P. and D.S. Su, *Recent Progress on the Growth Mechanism of Carbon Nanotubes: A Review*. Chemsuschem, 2011. **4**(7): p. 824-847.
75. Stadermann, M., Sherlock, S. P., In, J. B., Fornasiero, F., Park, H. G., Artyukhin, A. B., ... & Noy, A., *Mechanism and kinetics of growth termination in controlled chemical vapor deposition growth of multiwall carbon nanotube arrays*. Nano letters, 9(2), 738-744, 2009.
76. Puretzky, A.A., Geohegan, D. B., Jesse, S., Ivanov, I. N., & Eres, G., *In situ measurements and modeling of carbon nanotube array growth kinetics during chemical vapor deposition*. Applied Physics A, 81(2), 223-240, 2005.
77. Kamachali, R.D., *Theoretical calculations on the catalytic growth of multiwall carbon nanotube in chemical vapor deposition*. Chemical physics, 327(2), 434-438, 2006.
78. Patole, S.P., Kim, H., Choi, J., Kim, Y., Baik, S., & Yoo, J. B., *Kinetics of catalyst size dependent carbon nanotube growth by growth interruption studies*. Applied Physics Letters, 96(9), 094101, 2010.
79. Pal, S.K., Talapatra, S., Kar, S., Ci, L., Vajtai, R., Borca-Tasciuc, T., ... & Ajayan, P. M., *Time and temperature dependence of multi-walled carbon nanotube growth on Inconel 600*. Nanotechnology, 19(4), 045610, 2008.
80. Meshot, E.R., & Hart, A. J., *Abrupt self-termination of vertically aligned carbon nanotube growth*. Applied Physics Letters, 92(11), 113107, 2008.
81. Hasegawa, K., & Noda, S., *Millimeter-tall single-walled carbon nanotubes rapidly grown with and without water*. Acs Nano, 5(2), 975-984, 2011.

82. Louchev, O.A., Laude, T., Sato, Y., & Kanda, H., *Diffusion-controlled kinetics of carbon nanotube forest growth by chemical vapor deposition*. The Journal of chemical physics, 118(16), 7622-7634, 2003.
83. Christen, H.M., Poretzky, A. A., Cui, H., Belay, K., Fleming, P. H., Geohegan, D. B., & Lowndes, D. H., *Rapid growth of long, vertically aligned carbon nanotubes through efficient catalyst optimization using metal film gradients*. Nano Letters, 4(10), 1939-1942, 2004.
84. Liu, K., Jiang, K., Wei, Y., Ge, S., Liu, P., & Fan, S., *Controlled termination of the growth of vertically aligned carbon nanotube arrays*. Advanced Materials, 19(7), 975-978, 2007.
85. Xiang, R., Yang, Z., Zhang, Q., Luo, G., Qian, W., Wei, F., ... & Maruyama, S., *Growth deceleration of vertically aligned carbon nanotube arrays: Catalyst deactivation or feedstock diffusion controlled?* The Journal of Physical Chemistry C, 112(13), 4892-4896, 2008.
86. Mora, E., & Harutyunyan, A. R., *Study of single-walled carbon nanotubes growth via the catalyst lifetime*. The Journal of Physical Chemistry C, 112(13), 4805-4812, 2008.
87. Zhu, L., et al., *The growth of carbon nanotube stacks in the kinetics-controlled regime*. Carbon, 2007. **45**(2): p. 344-348.
88. Hofmann, S., Csanyi, G., Ferrari, A. C., Payne, M. C., & Robertson, J., *Surface diffusion: the low activation energy path for nanotube growth*. Physical review letters, 95(3), 036101, 2005.
89. Pelech, I. and U. Narkiewicz, *The Kinetics of Ethylene Decomposition on Iron Catalyst*. Acta Physica Polonica A, 2009. **116**: p. S146-S149.
90. Yamada, T., et al., *Revealing the Secret of Water-Assisted Carbon Nanotube Synthesis by Microscopic Observation of the Interaction of Water on the Catalysts*. Nano Letters, 2008. **8**(12): p. 4288-4292.
91. Stadermann, M., et al., *Mechanism and Kinetics of Growth Termination in Controlled Chemical Vapor Deposition Growth of Multiwall Carbon Nanotube Arrays*. Nano Letters, 2009. **9**(2): p. 738-744.
92. Borjesson, A. and K. Bolton, *Modeling of Ostwald Ripening of Metal Clusters Attached to Carbon Nanotubes*. Journal of Physical Chemistry C, 2011. **115**(50): p. 24454-24462.
93. Amama, P.B., et al., *Influence of Alumina Type on the Evolution and Activity of Alumina-Supported Fe Catalysts in Single-Walled Carbon Nanotube Carpet Growth*. Acs Nano, 2010. **4**(2): p. 895-904.
94. Louchev, O.A., Y. Sato, and H. Kanda, *Growth mechanism of carbon nanotube forests by chemical vapor deposition*. Applied Physics Letters, 2002. **80**(15): p. 2752.
95. Han, J.H., et al., *A mechanochemical model of growth termination in vertical carbon nanotube forests*. Acs Nano, 2008. **2**(1): p. 53-60.
96. Lee, K.H., J.M. Cho, and W. Sigmund, *Control of growth orientation for carbon nanotubes*. Applied Physics Letters, 2003. **82**(3): p. 448-450.
97. Zhang, Y.G., et al., *Electric-field-directed growth of aligned single-walled carbon nanotubes*. Applied Physics Letters, 2001. **79**(19): p. 3155-3157.
98. [www.nanocomptech.com](http://www.nanocomptech.com). *miralon yarn overview*. 2016.

99. Behabtu, N., et al., *Strong, light, multifunctional fibers of carbon nanotubes with ultrahigh conductivity*. Science, 2013. **339**(6116): p. 182-6.
100. Tsentelovich, D.E., et al., *Influence of Carbon Nanotube Characteristics on Macroscopic Fiber Properties*. ACS Appl Mater Interfaces, 2017.
101. Alvarenga, J., et al., *High conductivity carbon nanotube wires from radial densification and ionic doping*. Applied Physics Letters, 2010. **97**(18).
102. Yang, Z.B., et al., *Dependence of structures and properties of carbon nanotube fibers on heating treatment*. Journal of Materials Chemistry, 2011. **21**(36): p. 13772-13775.
103. Matsumoto, N., et al., *Scalability of the Heat and Current Treatment on SWCNTs to Improve their Crystallinity and Thermal and Electrical Conductivities*. Nanoscale Res Lett, 2015. **10**: p. 220.
104. Zhao, Y., et al., *Iodine doped carbon nanotube cables exceeding specific electrical conductivity of metals*. Sci Rep, 2011. **1**: p. 83.
105. Janas, D., et al., *Iodine monochloride as a powerful enhancer of electrical conductivity of carbon nanotube wires*. Carbon, 2014. **73**: p. 225-233.
106. Wehenkel, D.J., et al., *Unforeseen high temperature and humidity stability of FeCl<sub>3</sub> intercalated few layer graphene*. Sci Rep, 2015. **5**: p. 7609.
107. Sundaram, R.M., K.K. Koziol, and A.H. Windle, *Continuous direct spinning of fibers of single-walled carbon nanotubes with metallic chirality*. Adv Mater, 2011. **23**(43): p. 5064-8.
108. Morelos-Gómez, A., et al., *High electrical conductivity of double-walled carbon nanotube fibers by hydrogen peroxide treatments*. J. Mater. Chem. A, 2016. **4**(1): p. 74-82.
109. Subramaniam, C., et al., *One hundred fold increase in current carrying capacity in a carbon nanotube-copper composite*. Nat Commun, 2013. **4**: p. 2202.
110. Lekawa-Raus, A., P. Haladyj, and K. Koziol, *Carbon nanotube fiber-silver hybrid electrical conductors*. Materials Letters, 2014. **133**: p. 186-189.
111. Lekawa-Raus, A., et al., *Electrical Properties of Carbon Nanotube Based Fibers and Their Future Use in Electrical Wiring*. Advanced Functional Materials, 2014. **24**(24): p. 3661-3682.
112. Lu, W.B., et al., *State of the Art of Carbon Nanotube Fibers: Opportunities and Challenges*. Advanced Materials, 2012. **24**(14): p. 1805-1833.
113. Zhang, X.F., et al., *Ultrastrong, stiff, and lightweight carbon-nanotube fibers*. Advanced Materials, 2007. **19**(23): p. 4198-+.
114. Jarosz, P.R., Shaukat, A., Schauerman, C. M., Cress, C. D., Kladitis, P. E., Ridgley, R. D., & Landi, B. J., *High-performance, lightweight coaxial cable from carbon nanotube conductors*. ACS applied materials & interfaces, 2012: p. 1103-1109.
115. Mirri, F., Orloff, N. D., Forster, A. M., Ashkar, R., Headrick, R. J., Bengio, E. A., ... & Butler, P., *Lightweight, flexible, high-performance carbon nanotube cables made by scalable flow coating*. ACS applied materials & interfaces, 2016: p. 4903-4910.
116. Talapatra, S., Kar, S., Pal, S. K., Vajtai, R., Ci, L., Victor, P., ... & Ajayan, P. M., *Direct growth of aligned carbon nanotubes on bulk metals*. Nature nanotechnology, 2006: p. 112-116.



117. Rahmat, M. and P. Hubert, *Carbon nanotube-polymer interactions in nanocomposites: A review*. Composites Science and Technology, 2011. **72**(1): p. 72-84.
118. Green, M.J., et al., *Nanotubes as polymers*. Polymer, 2009. **50**(21): p. 4979-4997.
119. Lucas, A., et al., *Kinetics of Nanotube and Microfiber Scission under Sonication*. Journal of Physical Chemistry C, 2009. **113**(48): p. 20599-20605.
120. Karousis, N., N. Tagmatarchis, and D. Tasis, *Current Progress on the Chemical Modification of Carbon Nanotubes*. Chemical Reviews, 2010. **110**(9): p. 5366-5397.
121. Duque, J.G., et al., *Diameter-Dependent Solubility of Single-Walled Carbon Nanotubes*. Acs Nano, 2010. **4**(6): p. 3063-3072.
122. Mazov, I., et al., *Oxidation behavior of multiwall carbon nanotubes with different diameters and morphology*. Applied Surface Science, 2012. **258**(17): p. 6272-6280.
123. Davis, V.A., et al., *True solutions of single-walled carbon nanotubes for assembly into macroscopic materials*. Nature Nanotechnology, 2009. **4**(12): p. 830-834.
124. Ryu, Y., L. Yin, and C.H. Yu, *Dramatic electrical conductivity improvement of carbon nanotube networks by simultaneous de-bundling and hole-doping with chlorosulfonic acid*. Journal of Materials Chemistry, 2012. **22**(14): p. 6959-6964.
125. Tristant, D., et al., *Enlightening the ultrahigh electrical conductivities of doped double-wall carbon nanotube fibers by Raman spectroscopy and first-principles calculations*. Nanoscale, 2016. **8**(47): p. 19668-19676.
126. Davis, V.A., et al., *Phase Behavior and rheology of SWNTs in superacids*. Macromolecules, 2004. **37**(1): p. 154-160.
127. Zhou, W., et al., *Single-walled carbon nanotube-templated crystallization of H2SO4: Direct evidence for protonation*. Journal of the American Chemical Society, 2005. **127**(6): p. 1640-1641.
128. Tantang, H., et al., *Using oxidation to increase the electrical conductivity of carbon nanotube electrodes*. Carbon, 2009. **47**(7): p. 1867-1870.
129. Green, M.J., et al., *Modeling the phase behavior of polydisperse rigid rods with attractive interactions with applications to single-walled carbon nanotubes in superacids*. Journal of Chemical Physics, 2009. **131**(8).
130. Lekawa-Raus, A., et al., *Towards the development of carbon nanotube based wires*. Carbon, 2014. **68**: p. 597-609.
131. Zhang, H., et al., *A Facile, Low-Cost, and Scalable Method of Selective Etching of Semiconducting Single-Walled Carbon Nanotubes by a Gas Reaction*. Advanced Materials, 2009. **21**(7): p. 813-816.
132. Nirmalraj, P.N., et al., *Electrical Connectivity in Single-Walled Carbon Nanotube Networks*. Nano Letters, 2009. **9**(11): p. 3890-3895.
133. Puchades, I., et al., *Mechanism of chemical doping in electronic-type-separated single wall carbon nanotubes towards high electrical conductivity*. Journal of Materials Chemistry C, 2015. **3**(39): p. 10256-10266.
134. Cho, W.D., M. Schulz, and V. Shanov, *Growth termination mechanism of vertically aligned centimeter long carbon nanotube arrays*. Carbon, 2014. **69**: p. 609-620.

135. Yasuda, S., et al., *Improved and Large Area Single-Walled Carbon Nanotube Forest Growth by Controlling the Gas Flow Direction*. *Acs Nano*, 2009. **3**(12): p. 4164-4170.
136. Lee, J., et al., *Impact of carbon nanotube length on electron transport in aligned carbon nanotube networks*. *Applied Physics Letters*, 2015. **106**(5).
137. Ericson, L.M., et al., *Macroscopic, neat, single-walled carbon nanotube fibers*. *Science*, 2004. **305**(5689): p. 1447-1450.
138. Halasz, G., et al., *Vortex flow generated by a magnetic stirrer*. *American Journal of Physics*, 2007. **75**(12): p. 1092-1098.
139. Tsentelovich, D.E., et al., *Relationship of Extensional Viscosity and Liquid Crystalline Transition to Length Distribution in Carbon Nanotube Solutions*. *Macromolecules*, 2016. **49**(2): p. 681-689.
140. Neri, W., et al., *Surfactant-free spinning of composite carbon nanotube fibers*. *Macromolecular Rapid Communications*, 2006. **27**(13): p. 1035-1038.
141. Li, Q.W., et al., *Structure-dependent electrical properties of carbon nanotube fibers*. *Advanced Materials*, 2007. **19**(20): p. 3358-+.
142. Behabtu, N., et al., *Strong, Light, Multifunctional Fibers of Carbon Nanotubes with Ultrahigh Conductivity*. *Science*, 2013. **339**(6116): p. 182-186.
143. Zhao, Y., et al., *Iodine doped carbon nanotube cables exceeding specific electrical conductivity of metals*. *Scientific Reports*, 2011. **1**.
144. Zhong, X.H., et al., *Continuous Multilayered Carbon Nanotube Yarns*. *Advanced Materials*, 2010. **22**(6): p. 692-+.
145. Zhou, W., et al., *Single wall carbon nanotube fibers extruded from super-acid suspensions: Preferred orientation, electrical, and thermal transport*. *Journal of Applied Physics*, 2004. **95**(2): p. 649-655.
146. John R. Ferraro, K.N.a.C.W.B., *Introductory Raman Spectroscopy* 2003: Elsevier.
147. Dresselhaus, M.S., et al., *Raman spectroscopy of carbon nanotubes*. *Physics Reports-Review Section of Physics Letters*, 2005. **409**(2): p. 47-99.
148. Heise, H.M., et al., *Characterisation of carbonaceous materials using Raman spectroscopy: a comparison of carbon nanotube filters, single- and multi-walled nanotubes, graphitised porous carbon and graphite*. *Journal of Raman Spectroscopy*, 2009. **40**(3): p. 344-353.
149. Rao, A.M., A. Jorio, M. A. Pimenta, M. S. S. Dantas, Riichiro Saito, G. Dresselhaus, and M. S. Dresselhaus, *Polarized Raman study of aligned multiwalled carbon nanotubes*. *Physical review letters*, 2000. **84**(8): p. 1820.
150. Duesberg, G.S., I. Loa, M. Burghard, K. Syassen, and S. Roth. , *Polarized Raman spectroscopy on isolated single-wall carbon nanotubes*. *Physical review letters*, 2000. **85**(25): p. 5436.
151. Gommans, H.H., et al., *Fibers of aligned single-walled carbon nanotubes: Polarized Raman spectroscopy*. *Journal of Applied Physics*, 2000. **88**(5): p. 2509-2514.